ENGINEERING EXPERIMENT STATION
of the Georgia Institute of Technology
Atlanta, Georgia

FINAL REPORT

PROJECT NO. 187

THE AVERAGE VALUE AND LONGITUDINAL GRADIENT OF THE INDUCED VELOCITY AT A HELICOPTER ROTOR OPERATING AT POSITIVE ANGLES OF ATTACK AS DETERMINED BY WIND TUNNEL FORCE TESTS OF A FOUR FOOT DIAMETER MODEL ROTOR

By

WALTER CASTLES, JR.
Daniel Guggenheim School of Aeronautics

o - o - o - o - o - o - o - o - o

CONTRACT NO. Naw-6092

NATIONAL ADVISORY COMMITTEE FOR AERONAUTICS

o - o - o - o - o - o - o - o - o - o

AUGUST, 1955

THE AVERAGE VALUE AND LONGITUDINAL GRADIENT OF THE INDUCED VELOCITY AT A HELICOPTER ROTOR OPERATING AT POSITIVE ANGLES OF ATTACK AS DETERMINED BY WIND TUNNEL FORCE TESTS OF A FOUR FOOT DIAMETER MODEL ROTOR

Prepared by _____
Walter Castles, Jr., Assoc. Prof.
Daniel Guggenheim School of
Aeronautics

Approved by _____
for Donnell W. Dutton, Director
Daniel Guggenheim School of
Aeronautics

Released by _____
Paul K. Calaway, Director
Engineering Experiment Station

August, 1955

TABLE OF CONTENTS

TABLE OF CONTENTS (CONTINUED)

TABLE OF CONTENTS (CONTINUED)

Page

THE AVERAGE VALUE AND LONGITUDINAL GRADIENT OF THE INDUCED VELOCITY AT A HELICOPTER ROTOR OPERATING AT POSITIVE ANGLES OF ATTACK AS DETERMINED BY WIND TUNNEL FORCE TESTS OF A FOUR FOOT DIAMETER MODEL ROTOR

By Walter Castles, Jr.

Georgia Institute of Technology

SUMMARY

The survey test program covered in this report was conducted in an attempt to determine the positive rotor angle of attack flight ranges wherein existing induced flow theory was adequate and the flight ranges where the theory was in need of improvement.

The average value and longitudinal gradient of the normal component of induced velocity at a helicopter rotor was computed from the results of wind tunnel force tests on a four-foot diameter two-bladed model rotor with a solidity of 0.05. The tests were run at $C_T = 0.0040$ and covered the whole positive rotor angle of attack range from approximately zero rotor angle of attack to autorotation and from $\mu_v = 0$ to $\mu_v = 0.50$.

The values of the average nondimensional induced velocity λ_i were independently computed by means of a rotor thrust equation and a simplified rotor torque equation using measured values of the parameters. The values of the nondimensional longitudinal induced velocity gradient w were computed by use of the equation for the lateral flapping angle coefficient b_1.

The computed values of λ_i and w that are presented in this report would not necessarily agree with mean values obtained by direct velocity measurements since the inverse errors of the rotor thrust, torque, or blade flapping angle equations (i.e. neglect of blade stall, nonlinear induced velocity gradients, etc.) are included in the present results.

A comparison, by means of surface plots, of the experimentally derived values of the nondimensional mean induced velocity λ_i with the values given by contemporary induced flow theory, which is based upon the assumption of a uniform semi-infinite elliptic wake-vortex-cylinder, indicates that present theory is inadequate to describe the induced flow at steep angles of power-on descent. The comparison also indicates that present theory underestimates the mean induced velocity in the high-speed flight range although the largest part of the discrepancies at the higher values of the speed ratio μ probably arise from the direct effects of blade stall.

The experimental and theoretical values of the nondimensional mean longitudinal induced velocity gradient w are in reasonable agreement except for a small region around the point at $\mu_v = \lambda_v = 0$ where the theory gives a singular infinite value.

The results of the vertical descent test points obtained in the present investigation appear to indicate that the power unstable (i.e. $\frac{d\lambda_i}{d\lambda_z} > 1$) vertical descent range is less extensive for a two bladed rotor than for the similar three bladed rotor of TN 2474.

Photographs were taken, at each test point, of a tuft grid located on the longitudinal center-line plane of the rotor. A series of sketches are given of the tuft patterns in the longitudinal center-plane for vertical and inclined descent.

The region of rough flow was approximately determined by noting at which test points there were oscillations in the rotor thrust and/or irregular flapping motion of the blades.

INTRODUCTION

As contemporary induced flow theory is based upon the assumption that the wake vortex system consists of a uniform, semi-infinite, elliptic vortex-cylinder, the accuracy of the theory has appeared to be questionable for those partial-power inclined descent flight conditions where the wake may be of abnormal type. The test program which forms the basis of the present report was undertaken to survey the positive rotor angle of attack flight regime in an attempt to determine the flight ranges for which present induced flow theory is useful and the flight ranges for which it is unsatisfactory.

NOTATION

a	slope of lift curve for blade element at $r = 0.75\ R$
a_o	rotor coning angle
a_1	longitudinal blade flapping angle coefficient
A_o	mean blade pitch angle at $r = 0.75\ R$
b	number of blades in rotor
b_1	lateral blade flapping angle coefficient
c	blade chord at radius r
$\bar{c}$	mean blade chord $\dfrac{\int_o^R c\, r^2\, dr}{\int_o^R r^2\, dr}$
c_{d_o}	section profile-drag coefficient
c_l	section lift coefficient
C_Q	rotor torque coefficient $\left(\dfrac{Q}{\rho\, \pi\, \Omega^2\, R^5}\right)$
ΔC_Q	increment in rotor torque coefficient above that for zero thrust and freestream velocity
C_T	rotor thrust coefficient $\left(\dfrac{T}{\rho\, \pi\, \Omega^2\, R^4}\right)$
I_{nc}	$\sigma_{nc} \sin A_o + \sigma_{ns} \cos A_o$
I_{ns}	$\sigma_{ns} \sin A_o - \sigma_{nc} \cos A_o$
Q	rotor torque
r	radius of blade element $c\ dr$
R	rotor radius

T rotor thrust (component of rotor force that is normal to the plane of rotation or tip-path plane)

v mean normal component of induced velocity over the rotor disk

V freestream velocity

V_i normal component of induced velocity at r, ψ

w slope of longitudinal variation of nondimensional induced velocity

(i.e. $\frac{V_i}{\Omega R} = -\frac{v}{\Omega R} + w x \cos\psi + y x \sin\psi$)

x nondimensional blade radius r/R

x_1 nondimensional radius of inboard blade element

α angle of attack of plane of zero feathering

α_v angle of attack of tip-path plane ($\alpha + a_1$)

δ_o value of c_{d_o} at $c_l = 0$

ε constant in power equation for c_{d_o} (i.e. $c_{d_o} = \delta_o + \varepsilon c_l^2$)

λ_v mean inflow velocity ratio for rotor disk ($\frac{V \sin \alpha_v - v}{\Omega R}$)

μ_v in-plane velocity ratio for tip-path plane ($\frac{V \cos \alpha_v}{\Omega R}$)

ρ air density

$\sigma = \frac{b \bar{c}}{\pi R}$ rotor solidity

$\sigma_{nc} = \frac{1}{\pi R} \int_{x_1}^{1} c \cos\theta_t \; x^{n-1} \, dx$

$\sigma_{ns} = \frac{1}{\pi R} \int_{x_1}^{1} c \sin\theta_t \; x^{n-1} \, dx$

} constants which express blade chord and twist, θ_t

ψ azimuth angle of reference rotor blade measured from the downwind direction

Ω angular velocity of rotor

λ_i nondimensional mean induced velocity

$$\left(\lambda_i = \frac{v}{\Omega R} \sqrt{\frac{2 - 3 \mu_v^2}{C_T}} \right)$$

λ_x nondimensional inplane component of flight path velocity

$$\left(\lambda_x = \mu_v \sqrt{\frac{2 - 3 \mu_v^2}{C_T}} \right)$$

λ_z nondimensional normal component of flight path velocity

$$\left(\lambda_z = \frac{V \sin (\alpha + a_1)}{\Omega R} \sqrt{\frac{2 - 3 \mu_v^2}{C_T}} \right)$$

DESCRIPTION OF APPARATUS

Wind Tunnel

The open-jet wind tunnel configuration used for the present tests was the same as described in reference 1, with the exception of the addition of a ground plane (i.e. side-wall) spanning the side of the open-jet and located at the proper distance from the axis to make the open-jet wind tunnel wall correction essentially zero for a lifting line coinciding with the lateral diameter of the rotor. The side-wall served the additional purpose of confining the rotor wake within the tunnel boundaries and thus prevented the tunnel flow oscillations which would have otherwise resulted for some test conditions from the splitting of the rotor wake by the lip of the wind tunnel exit cone.

Rotor Test Stand

The rotor test stand was that described in reference 1 with modifications in the drive system to allow the wind tunnel balance yaw mechanism to be used to set and measure the rotor angle of attack and a modification in the hub assembly to accommodate the teetering model rotor. In addition, three micrometer type electrical feeler contacts were installed on the outside of the housing at $\psi = 0$, 90°, and 270° to measure the rotor flapping angles. The extension of these feelers, which contacted machined surfaces on the blade roots to light neon glow lamps, was measured and operated by autosyns coupled to counters. The feelers were kept in the retracted position except for momentary extension to the contact position at the time a flapping angle measurement was being made.

Model Rotor

The model rotor was a two-bladed teetering type with over 20° flapping freedom. The solidity was $\sigma = 0.05$ and the blades had a 2/1 taper and an NACA 43015 airfoil section. This airfoil section was used in order to obtain more nearly full-scale maximum lift coefficients than could be obtained from the usual rotor airfoils at the low test Reynold's numbers. The blades were constructed with a steel leading edge and laminated walnut trailing edge similar to the tapered blades shown in reference 1.

Tuft Grid

The tuft grid was located in the longitudinal rotor center-plane and rotated with the rotor plane of zero feathering. The tufts were spaced on 6 inch centers and covered a circle of approximately four foot radius about the rotor hub. The test set-up is shown in figure 1.

TEST PROCEDURE

The freestream velocity (i.e. wind tunnel fan rpm), rotor rpm, and rotor thrust were held constant for each test run, and measurements were made of the rotor torque, mean blade angle, and flapping angles at a series of settings of the angle of attack of the plane of zero feathering covering the range from -5° to an angle which yielded a negative torque coefficient.

The operating procedure was essentially the same as reported in reference 1 with the exception of the additional measurements of the rotor angles of attack and flapping angles.

REDUCTION OF DATA

The mean nondimensional value of the normal component of induced velocity λ_i at the plane of rotation of the rotor was computed from the test data by two independent methods.

The first method consisted of computing the values of λ_v, $\frac{V}{\Omega R}$, and λ_i using the blade element thrust equation of reference 2 and measured values of the parameters. After neglecting small terms and the coning angle a_o, which was essentially zero for the very heavy teetering model rotor with zero initial cone, the equations reduced to

$$\lambda_v = \frac{I_{3c} + \frac{1}{2}\mu_v^2 I_{1c} + a_1 \mu_v I_{2s} - \frac{2 C_T}{a b}}{I_{2s} - \frac{1}{2} a_1 \mu_v I_{1c}} \tag{1}$$

$$\frac{V}{\Omega R} = \frac{V}{\Omega R} \sin (\alpha + a_1) - \lambda_v \tag{2}$$

$$\lambda_i = \frac{V}{\Omega R} \sqrt{\frac{2 - 3\mu_v^2}{C_T}} \tag{3}$$

where, for the model rotor with zero blade twist operating at small blade angles,

$$I_{nc} = A_o \sigma_{nc}$$

$$I_{ns} = \sigma_{nc}$$

$$\sigma_{nc} = \frac{1}{\pi R} \int_{x_1}^{1} c\, x^{n-1}\, dx$$

and

μ_v = $\frac{V}{\Omega R} \cos (\alpha + a_1)$

A_o = mean blade angle

R = rotor radius

c = blade chord at radius r

x = $\frac{r}{R}$

V = freestream velocity

Ω = angular velocity of rotor

α = angle of attack of plane of zero feathering

a_1 = longitudinal flapping angle coefficient

C_T = rotor thrust coefficient ($T/\rho \pi \Omega^2 R^4$)

a = slope of blade airfoil lift curve

b = number of blades

v = mean value of normal component of induced velocity over the rotor disk

The mean blade angle A_o was obtained by reducing the values measured at the blade root by a factor to allow for the calculated dynamic blade twist at the 3/4 radius station. The reduction factor was 2.5% for the 1200 rpm runs.

The values of the constants for the model rotor are given in Table 1.

The second method of computing λ_i from the test data was by use of the torque equation of reference 2 for a rotor with triangular blade

circulation distribution (i.e. approximately triangular loading). This torque equation was used rather than the blade element torque equation in order to simplify the data reduction and eliminate the blade angle A_o as a parameter.

Upon dropping second order terms the value of λ_v obtained from the torque equation was

$$\lambda_v = \frac{1}{2} C_T \mu_v + \frac{1}{8} \delta_o \left(\frac{\sigma}{C_T} \right) \mu_v^2 \left(1 - \mu_v^2 \right) + \frac{9}{2} \varepsilon \left(\frac{C_T}{\sigma} \right) \left(1 + \frac{8}{9} \mu_v^2 \right) - \left(1 - \mu_v^2 \right) \left(\frac{\Delta C_Q}{C_T} \right) \tag{4}$$

where

$$c_{d_o} = \delta_o + \varepsilon c_l^2$$

and

$$\Delta C_Q = C_Q - (\text{value of } C_Q \text{ for zero thrust and freestream velocity})$$

The values of the average nondimensional longitudinal gradient w of the normal component of induced velocity at the plane of rotation were computed from the equation for the lateral flapping angle coefficient b_1 given in reference 2. Upon neglecting the coning angle term which was negligible for the model rotor, the resulting equation for w was

$$w = -b_1 \left(1 + \lambda_v \frac{I_{3c}}{I_{4s}} + \frac{1}{4} \mu_v^2 \frac{I_{2s}}{I_{4s}} \right) \tag{5}$$

RESULTS

The experimental values of the parameters and resultant calculated values of λ_i and w are given in tables 2 through 18. The tables also include the computed values of the nondimensional inplane and normal components of the freestream velocity λ_x and λ_z where

$$\lambda_x = \mu_v \frac{\sqrt{2 - 3\mu_v^2}}{C_T} \tag{6}$$

$$\lambda_z = \frac{V \sin(\alpha + a_1)}{\Omega R} \sqrt{\frac{2 - 3\mu_v^2}{C_T}} \tag{7}$$

The form of the equations for the nondimensional velocity ratios arises from the dependence of the values of the mean induced velocity ratio $\frac{v}{\Omega R}$ from reference 3 expressed in reference 2 as

$$\frac{v}{\Omega R} = \frac{\frac{1}{2} C_T}{(1 - \frac{3}{2}\mu_v^2)\sqrt{\mu_v^2 + \lambda_v^2}} \tag{8}$$

upon the $(1 - \frac{3}{2}\mu_v^2)$ term. This term represents the effect of the sinusoidal variation of blade bound vortex strength with ψ upon the mean wake-vortex-sheet strength. Equations 3, 6, and 7 follow from the reduction of equation 8 to the nondimensional form

$$\lambda_i = \sqrt{\frac{1}{\lambda_x^2 + (\lambda_z - \lambda_i)^2}} \tag{9}$$

It is to be noted that upon eliminating the radical, equation 9 becomes of the fourth order in λ_i and is multi-valued in the region near the end point of the windmill range.

The theoretical values of the nondimensional induced velocity λ_i from equation 9 are given in table 19 and shown in figure 2.

A comparison of the theoretical and experimental values of λ_i are shown in figure 3.

The theoretical values of w from the equation

$$w = -\frac{4}{3}\left(1 - 1.8\,\mu_v^2\right)\left[\sqrt{1 + \left(\frac{\lambda_v}{\mu_v}\right)^2} - \sqrt{\left(\frac{\lambda_v}{\mu_v}\right)^2}\right]\frac{v}{\Omega R} \qquad (10)$$

from reference 2 are given in table 20.

Figure 4 shows the comparison of the experimental and theoretical values of the mean nondimensional longitudinal induced velocity gradient w. It is seen from figure 4 that the theoretical values of w approach infinity at the ideal vertical autorotation point (i.e. $\mu_v = \lambda_v = 0$).

Figure 5 shows a sample tuft photograph.

Figures 6A through 6J show line drawings of the tuft patterns for vertical descent.

Figures 7A through 7E show the tuft patterns for inclined descent at $\frac{V}{\Omega R} = 0.07$.

Figures 8A through 8F show the tuft patterns for inclined descent at $\frac{V}{\Omega R} = 0.16$.

Figure 9 shows a plot of the flight region in which irregular variations in the model rotor thrust and blade flapping angles indicated

that the flow was unsteady.

Figure 10 shows a comparison of the values of λ_i versus λ_z in vertical descent for the two bladed rotor of the present program and the values from reference 1 for a similar three bladed rotor.

CONCLUDING REMARKS

The experimental results presented in this report include all the inverse errors of present rotor force theory. Consequently, for those flight conditions such as the high speed runs, where the effects of blade stall, nonlinear induced velocity gradients, etc., are large, the experimental values of λ_i must be considered to be qualitative in nature rather than quantitative.

Figure 2, a surface plot of the nondimensional induced velocity versus the nondimensional inplane and normal components of the flight path velocity, shows the discontinuity that exists in present induced flow theory. Although this discontinuity is outside the normal helicopter flight range, it appears from the test results shown in figure 3A that the validity of the present induced velocity equations may be questionable over a considerable flight range bordering on the discontinuity.

Figure 3B, a plot of the high speed runs, is probably more indicative of the large errors that arise from the neglect of blade stall and nonlinear induced velocity distribution effects on the mean computed blade angle and computed rotor torque than of any large error in the present methods of computing the mean induced velocity. Such errors are more apparent in the results of wind tunnel tests of bare rotors than in the results of flight tests which necessarily include the preponderant effects of parisite drag.

The comparison of the experimental and theoretical values of the mean nondimensional longitudinal induced velocity gradient w shown on figures 4A, 4B, and 4C indicates reasonably good agreement. The large theoretical gradients in the values of w near the ideal vertical descent autorotation point are apparently substantiated by the test results.

The line drawings of the tufts shown in figures 6, 7, and 8 give an indication of the flow directions in the region about the rotor. The lengths of the tuft arrows are not a true measure of the local velocities since the apparent length of the tuft was determined by the equilibrium inclination arising from the tuft drag and gravity forces. However, short tuft arrows indicate a region of very low velocity.

The vertical descent tuft drawings shown in figures 6A through 6J are for the flow on the open side of the tunnel as the flow was slightly unsymmetrical.

The tuft drawings (for the inclined descent conditions) shown in figures 7 and 8 include a region, in the upper left quadrant, in which the tufts were in the wake of the 6 inch diameter model hub and support tube. This region has been indicated by dotted lines.

The region of rough flow, for positive rotor angles of attack, insofar as it could be determined from fluctuations in the thrust and blade flapping angles of the very heavy model rotor, covers a band extending across the speed range of contemporary helicopters as shown by figure 9. It appears that the more severe high-speed roughness can be avoided by restricting inclined partial power descent to values of the speed ratio μ_v of less than 0.20 (i.e. λ_x less than 4).

A comparison of the vertical descent test results on the two bladed

rotor of the present program with the results given in reference 1 for a similar three bladed rotor as shown by figure 10 indicates that the power-unstable range of vertical descent may be smaller for the two bladed rotor. The comparison also indicates that the rate of vertical descent for autorotation may be lower for the two bladed rotor. However, the above variations may arise primarily from the differences in maximum section lift coefficients between the NACA 43015 section of the two bladed rotor and the NACA 0012 section of the three bladed rotor and the consequent different inboard blade stall patterns.

REFERENCES

1. Castles, Walter, Jr., and Gray, Robin B.: Empirical Relation Between Induced Velocity, Thrust, and Rate of Descent of a Helicopter Rotor as Determined by Wind-Tunnel Tests on Four Model Rotors. NACA TN 2474, Oct. 1951.

2. Castles, Walter, Jr., and New, Noah C.: A Blade-Element Analysis for Lifting Rotors that is Applicable for Large Inflow and Blade Angles and any Reasonable Blade Geometry. NACA TN 2656, July 1952.

3. Drees, Meijer, Jr.: A Theory of Airflow Through Rotors and It's Application to Some Helicopter Problems. The Journal of the Helicopter Association of Great Britain, Vol. 3, No. 2, July - August - Sept., 1949, pp. 79-104.

TABLE 1

CONSTANTS FOR UNTWISTED, TWO BLADED, TEETERING MODEL ROTOR

Radius	= 2'
Solidity	= 0.050
Airfoil section	= NACA 43015
Slope of lift curve	= 5.83/radian (estimated)
Profile drag coefficient c_{d_o}	= $0.012 + 0.030\ c_l^2$ (estimated)

Taper ratio of 2/1 between extended blade root chord of 3.016" and tip chord of 1.508"

Inboard blade airfoil radius = 4.50" (i.e. $x_1 = 0.187$)

σ_{1c} = 0.02286

σ_{2c} = 0.01268

σ_{3c} = 0.008256

σ_{4c} = 0.005991

TABLE 2

EXPERIMENTAL DATA - RUN # 2 (C_T = .00397, rpm = 1200)

$\frac{V}{\Omega R}$	α	A_o	a_1	b_1	ΔC_Q	μ_v	$(\lambda_v)_T$	$(\lambda_v)_Q$	w	λ_x	λ_z	$(\lambda_i)_T$	$(\lambda_i)_Q$
0.0195	0.000	0.155	0.0074	0.0068	0.000200	0.0195	-.047	-.039	-.007	0.437	0.003	0.90	0.88
0.0195	0.262	0.154	0.0060	0.0070	0.000197	0.0188	-.046	-.039	-.007	0.421	0.115	0.99	0.98
0.0195	0.523	0.154	0.0047	0.0096	0.000188	0.0168	-.046	-.036	-.010	0.377	0.220	1.10	1.03
0.0195	0.785	0.154	0.0038	0.0087	0.000193	0.0137	-.046	-.038	-.009	0.308	0.310	1.19	1.15
0.0195	1.047	0.155	0.0047	0.0053	0.000193	0.0097	-.047	-.038	-.005	0.217	0.379	1.28	1.22
0.0195	1.309	0.153	0.0072	0.0058	0.000182	0.0050	-.046	-.035	-.006	0.112	0.422	1.29	1.20
0.0195	1.571	0.157	0	0	0.000196	0	-.049	-.039	0	0	0.437	1.37	1.30

TABLE 3

EXPERIMENTAL DATA - RUN # 3 (C_T = .00400, rpm = 1200)

$\frac{V}{\Omega R}$	α	A_o	a_1	b_1	ΔC_Q	μ_v	$(\lambda_v)_T$	$(\lambda_v)_Q$	w	λ_x	λ_z	$(\lambda_i)_T$	$(\lambda_i)_Q$
0.0398	0.000	0.126	0.0171	0.0058	0.000176	0.0398	-.045	-.033	-.006	0.888	0.015	1.02	0.75
0.0398	0.262	0.122	0.0189	0.0089	0.000156	0.0382	-.041	-.028	-.009	0.853	0.246	1.17	0.87
0.0398	0.523	0.112	0.0114	0.0195	0.000127	0.0344	-.034	-.021	-.020	0.769	0.445	1.20	0.91
0.0418	0.785	0.115	-.0049	0.0189	0.000147	0.0297	-.037	-.026	-.019	0.663	0.656	1.48	1.23
0.0398	1.047	0.145	-.0047	0.0061	0.000233	0.0211	-.058	-.047	-.006	0.470	0.768	2.05	1.82
0.0398	1.309	0.145	-.0048	0.0054	0.000235	0.0105	-.057	-.048	-.005	0.234	0.858	2.14	1.92
0.0398	1.396	0.149	+.0034	0.0027	0.000241	0.0068	-.063	-.049	-.003	0.151	0.876	2.28	1.98
0.0398	1.483	0.142	-.0008	0.0065	0.000232	0.0035	-.058	-.047	-.006	0.078	0.886	2.17	1.94
0.0398	1.571	0.141	0	0	0.000221	0	-.057	-.044	0	0	0.889	2.17	1.88

TABLE 4

EXPERIMENTAL DATA - RUN # 4 (C_T = .00397, rpm = 1200)

$\frac{V}{\Omega R}$	α	A_o	a_1	b_1	ΔC_Q	μ_v	$(\lambda_v)_T$	$(\lambda_v)_Q$	w	λ_x	λ_z	$(\lambda_i)_T$	$(\lambda_i)_Q$
0.0597	0.000	0.150	0.0220	0.0370	0.000175	0.0597	-.042	-.033	-.037	1.335	0.029	0.96	0.76
0.0597	0.262	0.132	0.0113	0.0496	0.000121	0.0575	-.030	-.019	-.050	1.286	0.360	1.03	0.79
0.0597	0.523	0.102	-.0019	0.0526	0.000066	0.0517	-.011	-.006	-.053	1.159	0.666	0.91	0.79
0.0585	0.785	0.097	-.0048	0.0501	0.000056	0.0415	-.008	-.003	-.050	0.931	0.922	1.10	0.99
0.0585	1.047	0.115	+.0024	0.0496	0.000099	0.0291	-.019	-.014	-.050	0.653	1.137	1.57	1.45
0.0585	1.309	0.128	-.0022	0.0429	0.000153	0.0153	-.028	-.028	-.043	0.342	1.267	1.89	1.88
0.0569	1.396	0.128	+.0031	0.0268	0.000154	0.0097	-.028	-.028	-.027	0.217	1.258	1.88	1.88
0.0569	1.483	0.149	-.0018	0.0020	0.000192	0.0051	-.042	-.038	-.002	0.113	1.271	2.21	2.11
0.0565	1.571	0.149	0	0	0.000192	0	-.042	-.038	0	0	1.268	2.20	2.10

TABLE 5

EXPERIMENTAL DATA - RUN # 5 (C_T = .00404, rpm=1200)

$\frac{V}{\Omega R}$	α	A_o	a_1	b_1	ΔC_Q	μ_v	$(\lambda_v)_T$	$(\lambda_v)_Q$	w	λ_x	λ_z	$(\lambda_i)_T$	$(\lambda_i)_Q$
0.0772	0.000	0.139	0.0155	0.0182	0.000076	0.0772	-.036	-.008	-.018	1.708	0.026	0.81	-
0.0768	0.262	0.109	-.0007	0.0250	0.000070	0.0742	-.017	-.006	-.025	1.643	0.438	0.80	0.57
0.0756	0.523	0.079	-.0102	0.0226	0.000009	0.0658	+.002	+.009	-.022	1.459	0.823	0.77	0.62
0.0756	0.785	0.079	-.0116	0.0220	0.000012	0.0541	+.002	+.008	-.022	1.199	1.172	1.12	0.99
0.0752	1.047	0.074	-.0089	0.0295	0.000001	0.0382	+.006	+.011	-.029	0.848	1.439	1.30	1.19
0.0752	1.309	0.078	-.0083	0.0270	0.000007	0.0201	+.004	+.009	-.027	0.446	1.611	1.52	1.41
0.0752	1.571	0.084	0	0	0.000031	0	0	+.003	0	0	1.672	1.66	1.60

TABLE 6

EXPERIMENTAL DATA - RUN # 6 (C_T = .00413, rpm = 1200)

$\frac{V}{\Omega R}$	α	A_o	a_1	b_1	ΔC_Q	μ_v	$(\lambda_v)_T$	$(\lambda_v)_Q$	w	λ_x	λ_z	$(\lambda_i)_T$	$(\lambda_i)_Q$
0.0959	0.000	0.135	0.0318	0.0229	0.000127	0.0958	-.030	-.019	-.023	2.191	0.054	0.43	0.48
0.0959	0.262	0.095	0.0089	0.0251	0.000036	0.0924	-.006	+.003	-.025	2.020	0.560	0.72	0.50
0.0959	0.523	0.059	0.0062	0.0227	-.000041	0.0827	+.018	+.021	-.023	1.811	1.061	0.67	0.60
0.0967	0.785	0.033	0.0037	0.0259	-.000105	0.0681	+.034	+.036	-.026	1.494	1.505	0.75	0.70
0.0967	1.047	0.013	0.0032	0.0150	-.000154	0.0481	+.048	+.048	-.015	1.056	1.843	0.79	0.79
0.0975	1.309	0.002	0.0006	0.0101	-.000181	0.0252	+.054	+.055	-.010	0.553	2.071	0.87	0.86
0.1002	1.571	-.001	0	0	-.000194	0	+.055	+.053	0	0	2.206	0.99	1.15

TABLE 7

EXPERIMENTAL DATA - RUN # 7 (C_T = .00405, rpm = 1200)

$\frac{V}{\Omega R}$	α	A_o	a_1	b_1	ΔC_Q	μ_v	$(\lambda_v)_T$	$(\lambda_v)_Q$	w	λ_x	λ_z	$(\lambda_i)_T$	$(\lambda_i)_Q$
0.1178	0.000	0.129	0.0351	0.0207	0.000104	0.1177	-.027	-.014	-.021	2.590	0.090	0.68	0.39
0.1146	0.087	0.112	0.0278	0.0238	0.000071	0.1138	-.017	-.007	-.024	2.506	0.289	0.65	0.44
0.1146	0.174	0.098	0.0187	0.0245	0.000037	0.1125	-.008	+.002	-.025	2.477	0.484	0.65	0.53
0.1142	0.262	0.084	0.0118	0.0208	0.000003	0.1099	+.001	+.011	-.021	2.422	0.679	0.66	0.44
0.1140	0.349	0.069	0.0104	0.0205	-.000030	0.1067	+.010	+.019	-.020	2.352	0.884	0.65	0.38
0.1140	0.436	0.054	0.0105	0.0204	-.000062	0.1028	+.020	+.026	-.020	2.268	1.086	0.64	0.50

TABLE 8

EXPERIMENTAL DATA - RUN # 8 (C_T = .00405, rpm = 1200)

$\frac{V}{\Omega R}$	α	A_o	a_1	b_1	ΔC_Q	μ_v	$(\lambda_v)_T$	$(\lambda_v)_Q$	w	λ_x	λ_z	$(\lambda_i)_T$	$(\lambda_i)_Q$
0.1424	-.087	0.129	0.0457	0.0146	0.000144	0.1423	-.025	-.023	-.015	3.116	-.129	0.41	0.37
0.1428	0.000	0.126	0.0421	0.0156	0.000089	0.1427	-.023	-.010	-.016	3.125	0.131	0.64	0.35
0.1428	0.087	0.106	0.0318	0.0191	0.000044	0.1418	-.012	+.009	-.019	3.106	0.371	0.62	0.35
0.1428	0.174	0.094	0.0195	0.0169	0.000002	0.1402	-.006	+.011	-.017	3.070	0.603	0.72	0.35
0.1432	0.262	0.071	0.0184	0.0153	-.000043	0.1376	+.009	+.022	-.015	3.018	0.868	0.65	0.38
0.1432	0.349	0.049	0.0120	0.0133	-.000087	0.1340	+.023	+.033	-.013	2.939	1.110	0.59	0.39

TABLE 9

EXPERIMENTAL DATA - RUN # 9 (C_T = .00416, rpm = 1200)

$\frac{V}{\Omega R}$	α	A_o	a_1	b_1	ΔC_Q	μ_v	$(\lambda_v)_T$	$(\lambda_v)_Q$	w	λ_x	λ_z	$(\lambda_i)_T$	$(\lambda_i)_Q$
0.1619	-.087	0.129	0.0511	0.0109	0.000135	0.1618	-.022	-.021	-.011	3.475	-.125	0.34	0.32
0.1615	0.000	0.126	0.0468	0.0146	0.000079	0.1614	-.021	-.007	-.015	3.466	+.162	0.61	0.31
0.1615	0.087	0.105	0.0352	0.0150	0.000032	0.1603	-.009	+.004	-.015	3.444	+.423	0.61	0.33
0.1615	0.174	0.083	0.0258	0.0120	-.000022	0.1583	+.005	+.017	-.012	3.403	0.691	0.58	0.32
0.1615	0.262	0.061	0.0205	0.0120	-.000068	0.1551	+.019	+.028	-.012	3.337	0.968	0.56	0.37
0.1615	0.349	0.040	0.0156	0.0097	-.000119	0.1509	+.032	+.039	-.010	3.249	1.240	0.54	0.40

TABLE 10

EXPERIMENTAL DATA - RUN#10 (C_T = .00410, rpm = 1200)

$\frac{V}{\Omega R}$	α	A_o	a_1	b_1	ΔC_Q	μ_v	$(\lambda_v)_T$	$(\lambda_v)_Q$	w	λ_x	λ_z	$(\lambda_i)_T$	$(\lambda_i)_Q$
0.1790	-.087	0.143	0.0552	0.0070	0.000130	+.1790	-.032	-.019	-.007	3.854	-.123	0.56	0.27
0.1775	0.000	0.123	0.0487	0.0118	0.000070	+.1772	-.020	-.004	-.012	3.819	+.186	0.60	0.28
0.1763	0.087	0.100	0.0393	0.0113	0.000018	+.1748	-.006	+.008	-.011	3.770	0.479	0.60	0.31
0.1759	0.174	0.079	0.0292	0.0109	-.000037	+.1722	+.007	+.020	-.011	3.715	0.767	0.62	0.32
0.1755	0.262	0.055	0.0251	0.0085	-.000091	+.1683	+.022	+.033	-.009	3.635	1.073	0.59	0.34
0.1743	0.349	0.035	0.0167	0.0086	-.000138	+.1627	+.035	+.044	-.009	3.520	1.348	0.59	0.38

TABLE 11

EXPERIMENTAL DATA - RUN # 11 (C_T = .00411, rpm = 1200)

$\frac{V}{\Omega R}$	α	A_o	a_1	b_1	ΔC_Q	μ_v	$(\lambda_v)_T$	$(\lambda_v)_Q$	w	λ_x	λ_z	$(\lambda_i)_T$	$(\lambda_i)_Q$
0.1981	-.087	0.146	0.0644	0.0066	0.000133	0.1981	-.032	-.019	-.007	4.239	-.096	0.58	0.30
0.1966	0.000	0.123	0.0555	0.0088	0.000061	0.1963	-.018	-.002	-.009	4.202	+.233	0.61	0.27
0.1966	0.087	0.100	0.0451	0.0095	0.000002	0.1948	-.004	+.012	-.010	4.174	0.555	0.64	0.30
0.1958	0.174	0.072	0.0364	0.0063	-.000059	0.1914	+.013	+.026	-.006	4.105	0.879	0.59	0.32
0.1958	0.262	0.047	0.0281	0.0059	-.000120	0.1876	+.029	+.040	-.006	4.027	1.201	0.58	0.33
0.1954	0.349	0.022	0.0207	0.0050	-.000169	0.1822	+.043	+.052	-.005	3.917	1.518	0.58	0.40

TABLE 12

EXPERIMENTAL DATA - RUN # 12 (C_T = .00401, rpm = 1200)

$\frac{V}{\Omega R}$	α	A_o	a_1	b_1	ΔC_Q	μ_v	$(\lambda_v)_T$	$(\lambda_v)_Q$	w	λ_x	λ_z	$(\lambda_i)_T$	$(\lambda_i)_Q$
0.2149	-.087	0.147	0.0736	0.0063	0.000127	+.2148	-.032	-.017	-.006	4.627	-.062	0.62	0.29
0.2168	0.000	0.121	0.0643	0.0087	0.0000148	0.2164	-.015	+.001	-.009	4.658	0.299	0.63	0.27
0.2149	0.087	0.102	0.0580	0.0110	-.000013	0.2126	-.004	+.015	-.011	4.582	0.530	0.61	0.33
0.2149	0.174	0.067	0.0429	0.0053	-.000086	0.2098	+.017	+.033	-.005	4.526	0.999	0.63	0.28
0.2149	0.262	0.041	0.0317	0.0040	-.000147	0.2057	+.032	+.047	-.004	4.443	1.343	0.64	0.31
0.2149	0.349	0.018	0.0267	0.0040	-.000205	0.1999	+.047	+.061	-.004	4.326	1.706	0.68	0.37

TABLE 13

EXPERIMENTAL DATA - RUN # 13 (C_T = .00411, rpm = 1000)

$\frac{V}{\Omega R}$	α	A_o	a_1	b_1	ΔC_Q	μ_v	$(\lambda_v)_T$	$(\lambda_v)_Q$	w	λ_x	λ_z	$(\lambda_i)_T$	$(\lambda_i)_Q$
0.2588	-.087	0.158	0.1016	0.0081	0.000125	0.2587	-.030	-.016	-.008	5.416	+.077	0.71	0.41
0.2578	0.000	0.131	0.0920	0.0097	0.000031	0.2567	-.014	+.006	-.010	5.378	0.496	0.79	0.36
0.2578	0.087	0.099	0.0810	0.0068	-.000057	0.2542	+.006	+.026	-.007	5.331	0.905	0.78	0.34
0.2583	0.174	0.062	0.0616	0.0029	-.000161	0.2511	+.027	+.049	-.003	5.273	1.268	0.69	0.22
0.2573	0.262	0.029	0.0489	-	-.000234	0.2450	+.047	+.066	-	5.157	1.655	0.67	0.28
0.2559	0.349	0.003	0.0359	0.0002	-.000300	0.2372	+.062	+.082	000	5.008	2.029	0.72	0.30

TABLE 14

EXPERIMENTAL DATA - RUN # 14 (C_T = .00416, rpm = 800)

$\frac{V}{\Omega R}$	α	A_o	a_1	b_1	ΔC_Q	μ_v	$(\lambda_v)_T$	$(\lambda_v)_Q$	w	λ_x	λ_z	$(\lambda_i)_T$	$(\lambda_i)_Q$
0.3247	-.087	0.174	0.1433	0.0095	0.000087	0.3242	-.027	+.004	-.010	6.523	0.365	0.90	0.45
0.3217	0.000	0.137	0.1322	0.0128	-.000012	0.3189	-.004	+.017	-.013	6.436	0.856	0.92	0.51
0.3217	0.087	0.099	0.1146	0.0071	-.000125	0.3152	+.019	+.056	-.007	6.374	1.304	0.92	0.47
0.3199	0.174	0.059	0.0919	0.0041	-.000237	0.3086	+.041	+.065	-.004	6.264	1.709	0.87	0.37
0.3199	0.262	0.021	0.0716	0.0019	-.000315	0.3023	+.062	+.082	-.002	6.156	2.132	0.85	0.46
0.3217	0.349	-.008	0.0622	0.0060	-.000392	0.2949	+.080	+.100	-.006	6.028	2.629	0.99	0.58

TABLE 15

EXPERIMENTAL DATA - RUN # 15 (C_T = .00405, rpm = 600)

0.4289	-.087	0.191	0.2114	0.0168	0.000006	0.4256	-.010	+.014	-.019	8.069	1.007	1.20	0.72
0.4321	0.000	0.141	0.1787	0.0050	-.000184	0.4252	+.016	+.053	-.005	8.064	1.457	1.16	0.44
0.4289	0.087	0.097	0.1573	0.0049	-.000318	0.4162	+.041	+.081	-.005	7.954	1.985	1.19	0.43
0.4281	0.174	0.046	0.1241	0.0086	-.000456	0.4092	+.068	+.109	-.009	7.866	2.421	1.10	0.31
0.4281	0.262	0.001	0.0930	0.0064	-.000542	0.4015	+.091	+.128	-.007	7.766	2.872	1.11	0.40

TABLE 16

EXPERIMENTAL DATA - RUN # 16 (C_T = .00425, rpm = 400)

$\frac{V}{\Omega R}$	α	A_o	a_1	ΔC_Q	μ_v	$(\lambda_v)_T$	$(\lambda_v)_Q$	λ_x	λ_z	$(\lambda_i)_T$	$(\lambda_i)_Q$
0.6338	-.087	0.232	0.1821	-.000100	0.6310	-.060	+.034	8.685	0.826	1.64	0.35
0.6338	0.000	0.173	0.2037	-.000373	0.6207	+.011	+.074	8.744	1.806	1.64	0.76
0.6338	0.087	0.109	0.2326	-.000632	0.6017	+.090	+.115	8.821	2.922	1.60	1.99
0.6338	0.174	0.044	0.1865	-.000887	0.5930	+.126	+.155	8.841	3.338	1.46	1.78

TABLE 17

EXPERIMENTAL DATA - RUN #17 (C_T = .00412, λ_x = 0, rpm = 1200)

$\frac{V}{\Omega R}$	A_o	ΔCQ	$(\lambda_v)_T$	$(\lambda_v)_Q$	λ_z	$(\lambda_i)_T$	$(\lambda_i)_Q$
0.0000	0.162	0.000242	-.050	-.048	0	1.10	1.05
0.0195	0.156	0.000205	-.046	-.039	0.429	1.44	1.06
0.0418	0.164	0.000215	-.051	-.041	0.920	2.04	1.83
0.0581	0.138	0.000160	-.034	-.028	1.279	2.03	1.89
0.0768	0.071	-.000014	+.009	+.014	1.691	1.48	1.37

TABLE 18

EXPERIMENTAL DATA - RERUN # 17 (C_T = .00398, rpm = 1200)

$\frac{V}{\Omega R}$	A_o	ΔC_Q	$(\lambda_v)_T$	$(\lambda_v)_Q$	λ_z	$(\lambda_i)_T$	$(\lambda_i)_Q$
0	0.162	0.000247	-.052	-.062	0	1.16	1.14
0.0157	0.160	0.000220	-.050	-.044	0.352	1.48	1.34
0.0268	0.160	0.000192	-.050	-.037	0.602	1.73	1.43
0.0384	0.170	0.000169	-.057	-.032	0.860	2.13	1.57
0.0473	0.170	0.000250	-.057	-.052	1.061	2.33	2.22
0.0565	0.145	0.000169	-.041	-.032	1.266	2.18	1.97
0.0684	0.111	0.000079	-.019	-.009	1.533	1.94	1.73
0.0768	0.081	-.000009	+.001	+.013	1.721	1.69	1.42
0.0828	0.044	-.000089	+.025	+.033	1.855	1.29	1.09
0.0915	0.021	-.000154	+.040	+.049	2.051	1.15	0.94
0.0975	0	-.000166	+.054	+.052	2.184	0.98	1.00

TABLE 19

THEORETICAL VALUES OF λ_i

λ_x =	0	.2	.4	.6	.8	1.00	1.20	1.40	1.60	1.80	2.00
λ_z	λ_i										
0	1.000	0.991	0.961	0.914	0.854	0.786	0.715	0.648	0.586	0.533	0.486
0.2	1.105	1.093	1.057	1.000	0.924	0.842	0.756	0.677	0.606	0.547	0.494
0.4	1.220	1.205	1.162	1.092	1.000	0.897	0.792	0.698	0.619	0.554	0.500
0.6	1.344	1.325	1.275	1.189	1.070	0.947	0.820	0.712	0.625	0.556	0.500
0.8	1.477	1.455	1.395	1.290	1.150	0.984	0.833	0.713	0.621	0.552	0.494
1.0	1.618	1.594	1.521	1.369	1.210	1.000	0.824	0.698	0.613	0.539	0.485
1.2	1.766	1.737	1.651	1.495	1.250	0.976	0.789	0.668	0.582	0.520	0.470
1.4	1.920	1.863	1.790	1.589	1.220	0.896	0.727	0.627	0.550	0.496	0.452
1.6	2.080	2.046	1.929	1.662	1.000	0.769	0.654	0.577	0.518	0.472	0.432
1.8	2.246	2.205	2.084	1.000	0.767	0.659	0.585	0.529	0.483	0.445	0.410
2.0	$\frac{2.414}{1.000}$	0.979	0.785	0.704	0.630	0.574	0.526	0.484	0.450	0.418	0.389
2.2	0.642	0.634	0.610	0.589	0.543	0.509	0.476	0.444	0.418	0.392	0.369
2.4	0.537	0.532	0.519	0.503	0.481	0.457	0.433	0.410	0.390	0.371	0.349

TABLE 19

CONCLUDED

λ_x =	2.00	2.40	2.80	3.20	3.60	4.00	5.00	6.00	8.00	10.00
λ_z	λ_i									
0	0.486	0.410	0.354	0.310	0.278	0.250	0.200	0.167	0.125	0.100
.2	0.494	0.414	0.357	0.312	0.278	0.250	0.200	0.167	0.125	0.100
.4	0.500	0.416	0.357	0.312	0.278	0.250	0.200	0.167	0.125	0.100
.6	0.500	0.415	0.356	0.311	0.277	0.249	0.199	0.166	0.125	0.100
.8	0.494	0.413	0.352	0.309	0.276	0.248	0.198	0.166	0.125	0.100
1.0	0.485	0.404	0.347	0.306	0.272	0.246	0.197	0.165	0.124	0.100
1.2	0.470	0.395	0.341	0.301	0.269	0.243	0.196	0.164	0.124	0.099
1.4	0.452	0.384	0.333	0.295	0.265	0.240	0.195	0.163	0.124	0.099
1.6	0.432	0.370	0.325	0.289	0.260	0.237	0.192	0.162	0.123	0.099
1.8	0.410	0.357	0.315	0.282	0.256	0.233	0.191	0.161	0.122	0.099
2.0	0.389	0.344	0.305	0.275	0.250	0.228	0.188	0.159	0.122	0.099
2.2	0.369	0.329	0.295	0.267	0.245	0.224	0.186	0.158	0.121	0.098
2.4	0.349	0.315	0.285	0.261	0.239	0.210	0.184	0.156	0.120	0.097

TABLE 20

THEORETICAL VALUES OF w

μ_v =	0	.02	.05	.10	.15	.20	.25	.30	.35	.40	.45	.50
λ_v							− w					
0.16	0	.0009	.0022	.0036	.0042	.0043	.0041	.0038	.0034	.0030	.0009	.0003
0.14	0	.0012	.0029	.0045	.0051	.0050	.0047	.0043	.0038	.0033	.0012	.0006
0.12	0	.0017	.0039	.0058	.0062	.0058	.0053	.0048	.0042	.0037	.0016	.0009
0.10	0	.0025	.0054	.0074	.0074	.0068	.0061	.0054	.0047	.0042	.0019	.0013
0.08	0	.0039	.0079	.0097	.0090	.0079	.0069	.0060	.0052	.0045	.0023	.0016
0.06	0	.0067	.0122	.0127	.0108	.0091	.0077	.0066	.0057	.0049	.0026	.0019
0.04	0	.0140	.0198	.0165	.0129	.0104	.0086	.0072	.0062	.0054	.0030	.0022
0.02	0	.0390	.0334	.0213	.0152	.0117	.0095	.0079	.0067	.0058	.0034	.0026
0		.1333	.0533	.0266	.0176	.0132	.0104	.0086	.0073	.0062	.0038	.0029
-.02	0	.0390	.0334	.0213	.0152	.0117	.0095	.0079	.0067	.0058	.0034	.0026
-.04	0	.0140	.0198	.0165	.0129	.0104	.0086	.0072	.0062	.0054	.0030	.0022
-.06	0	.0067	.0122	.0127	.0108	.0091	.0077	.0066	.0057	.0049	.0026	.0019

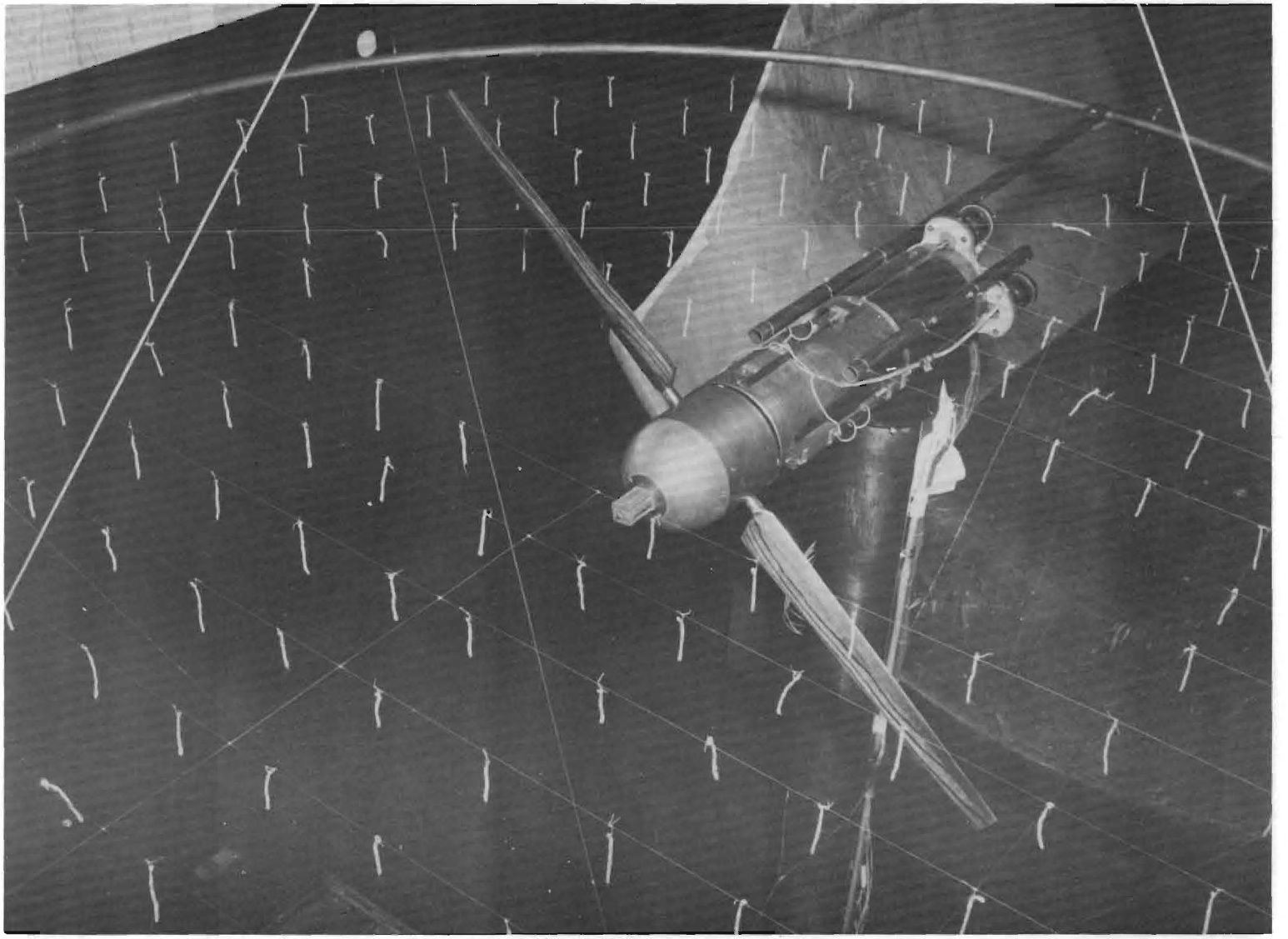

Figure 1. Test Configuration.

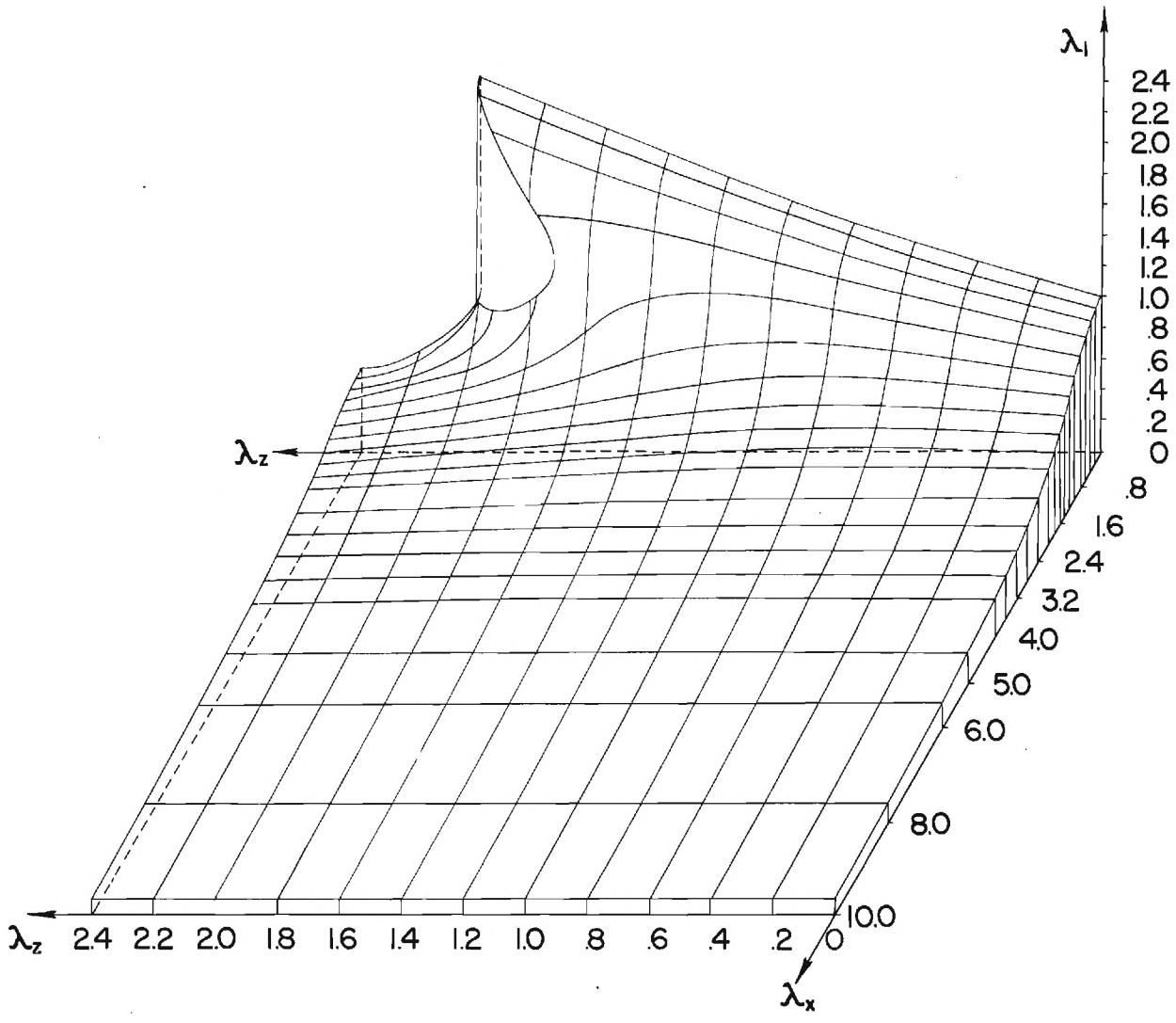

Figure 2. Theoretical Values of λ_i.

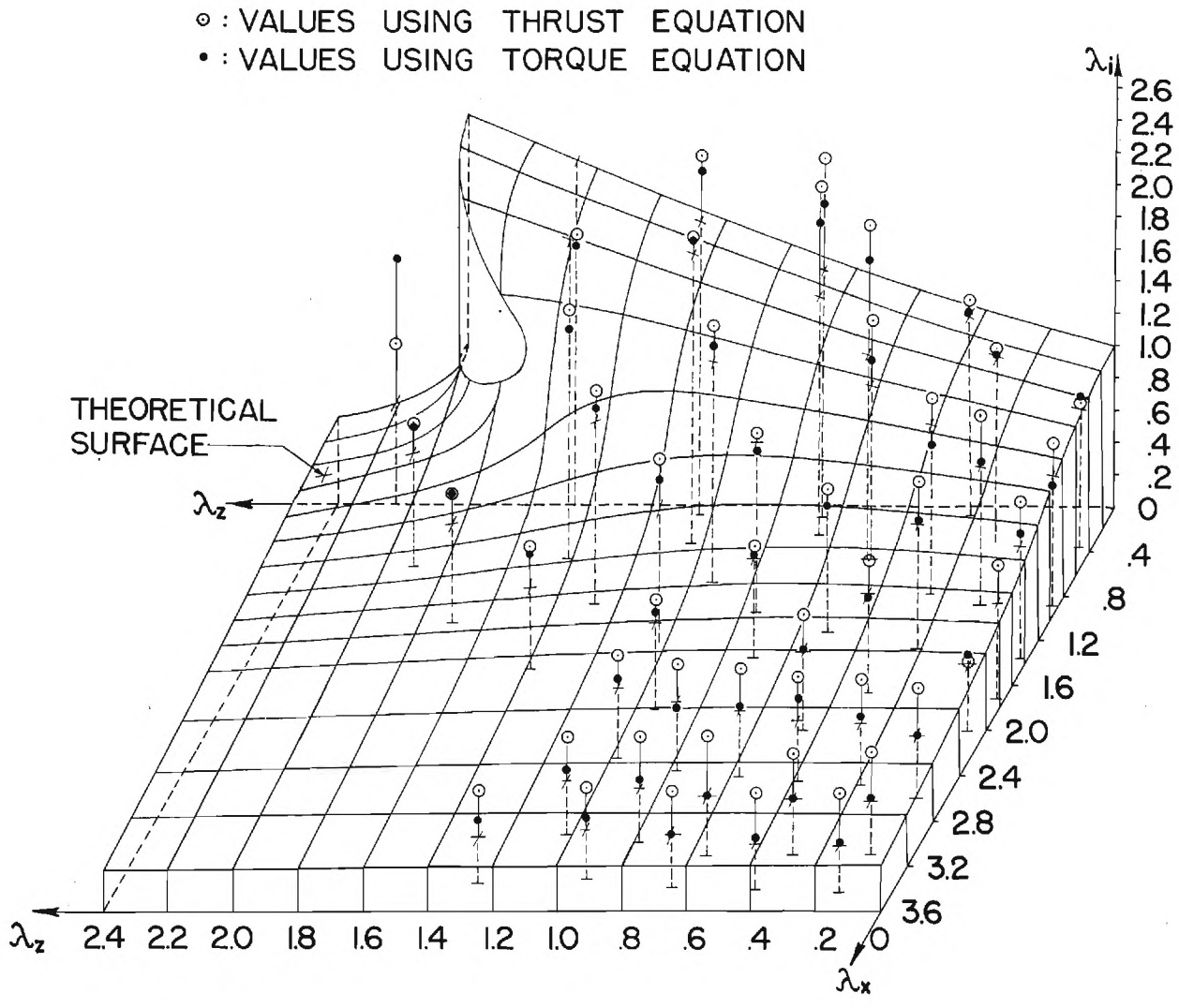

Figure 3A. Comparison of Theoretical and Experimental Values of λ_i for $\lambda_x < 3.6$.

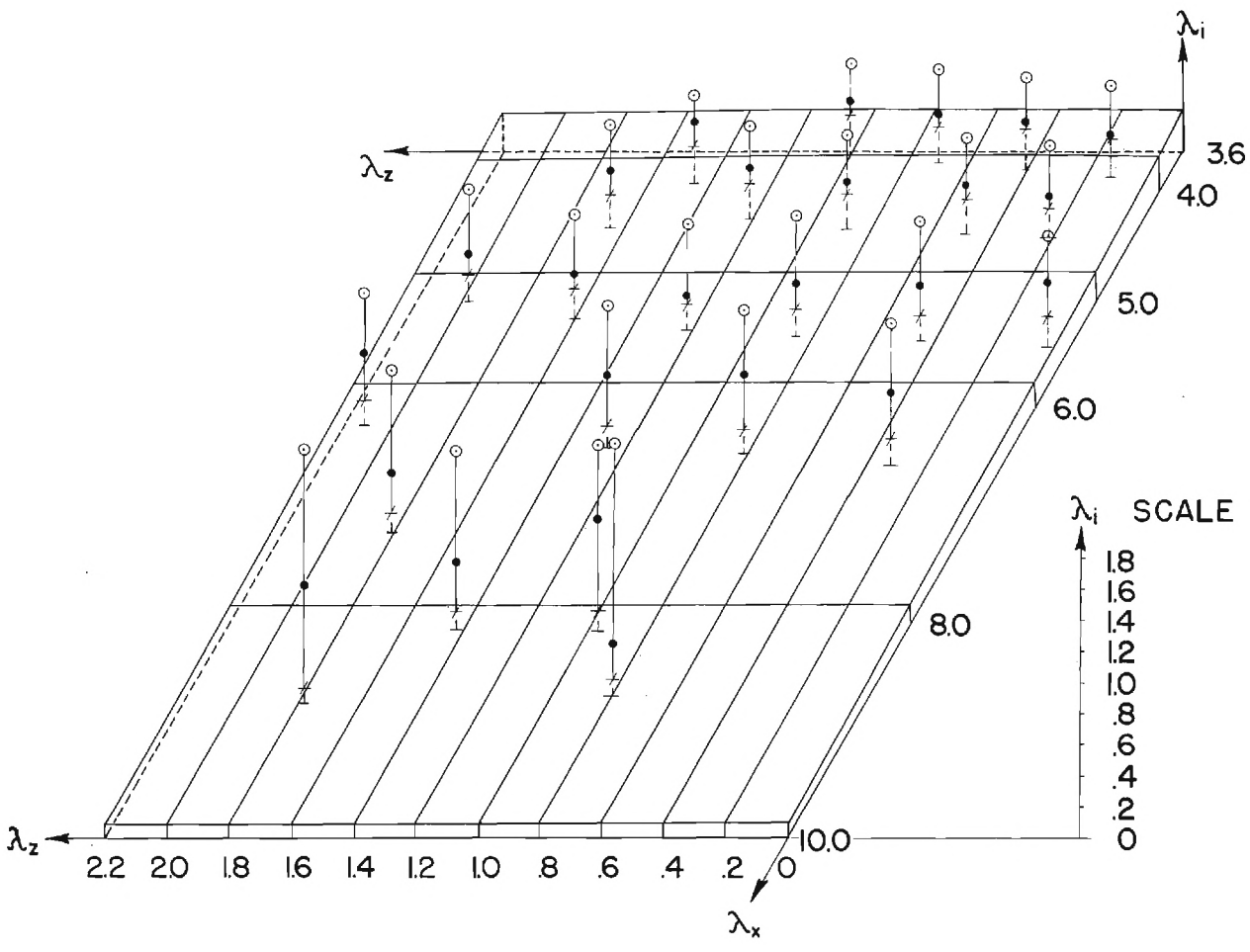

Figure 3B. Comparison of Theoretical and Experimental Values of λ_i for $\lambda_x > 3.6$.

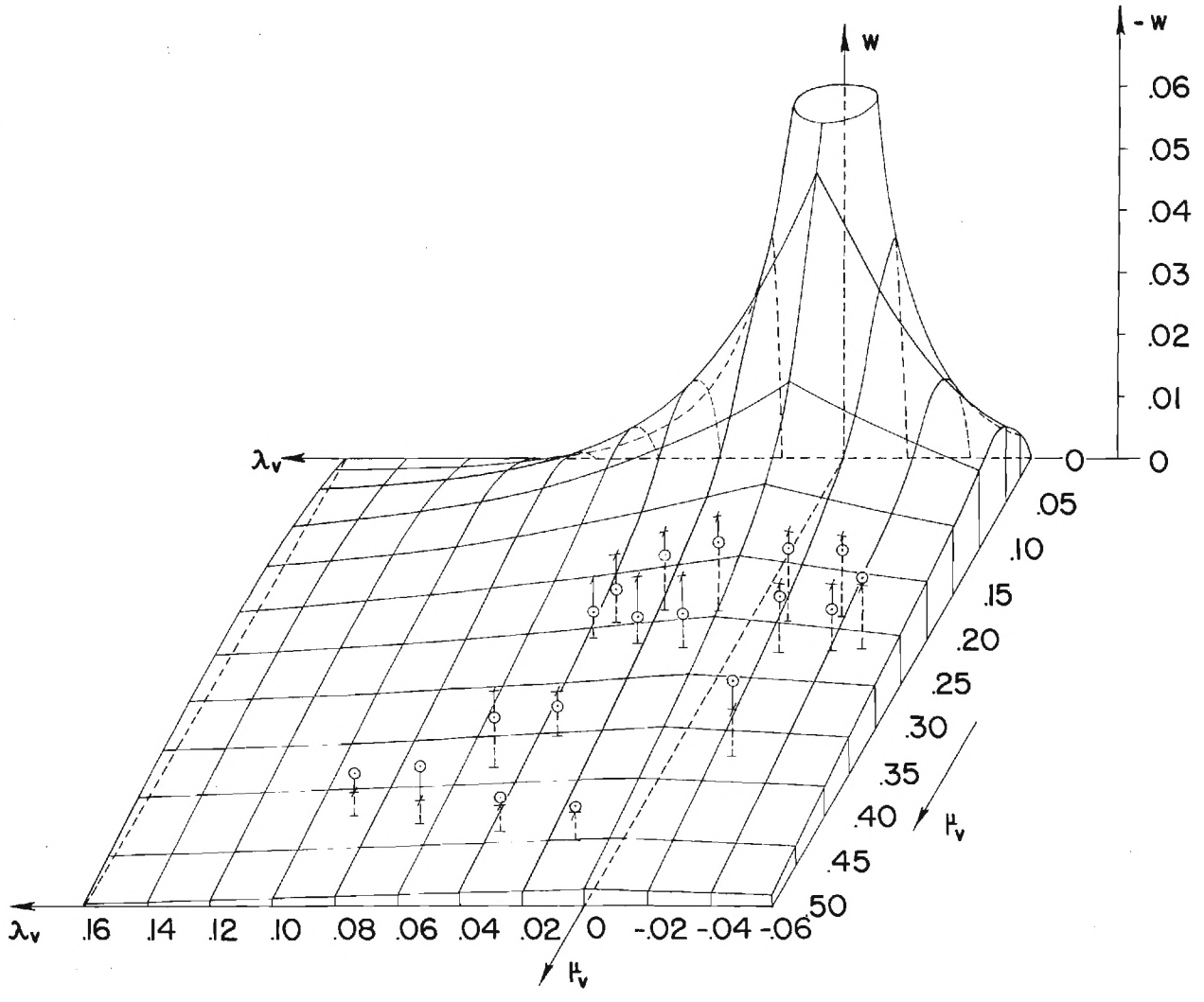

Figure 4A. Comparison of Theoretical and Experimental Values of w for $\mu_v > 1.5$.

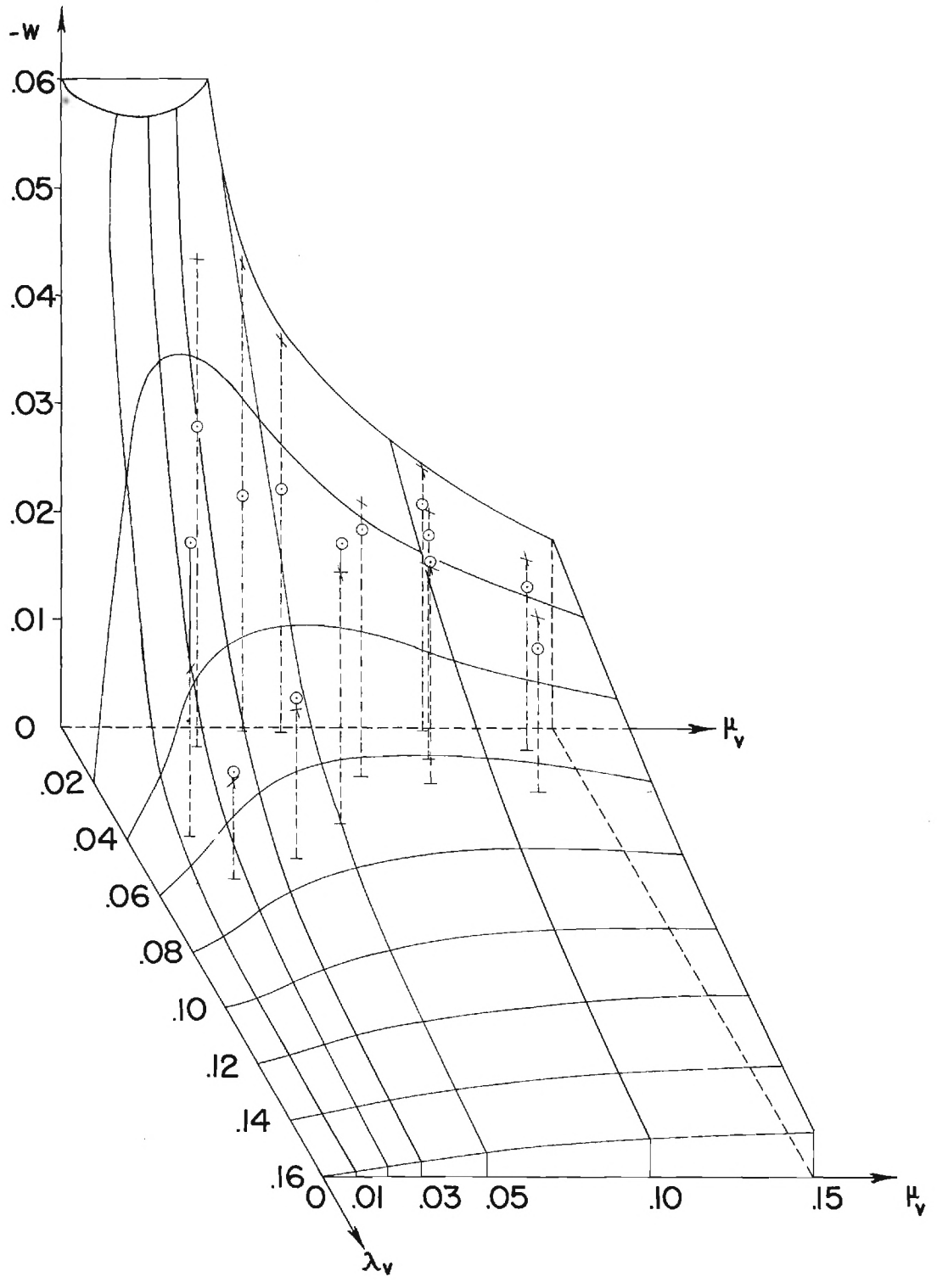

Figure 4B. Comparison of Theoretical and Experimental Values of w for $\mu_v < 1.5$, $\lambda_v > 0$.

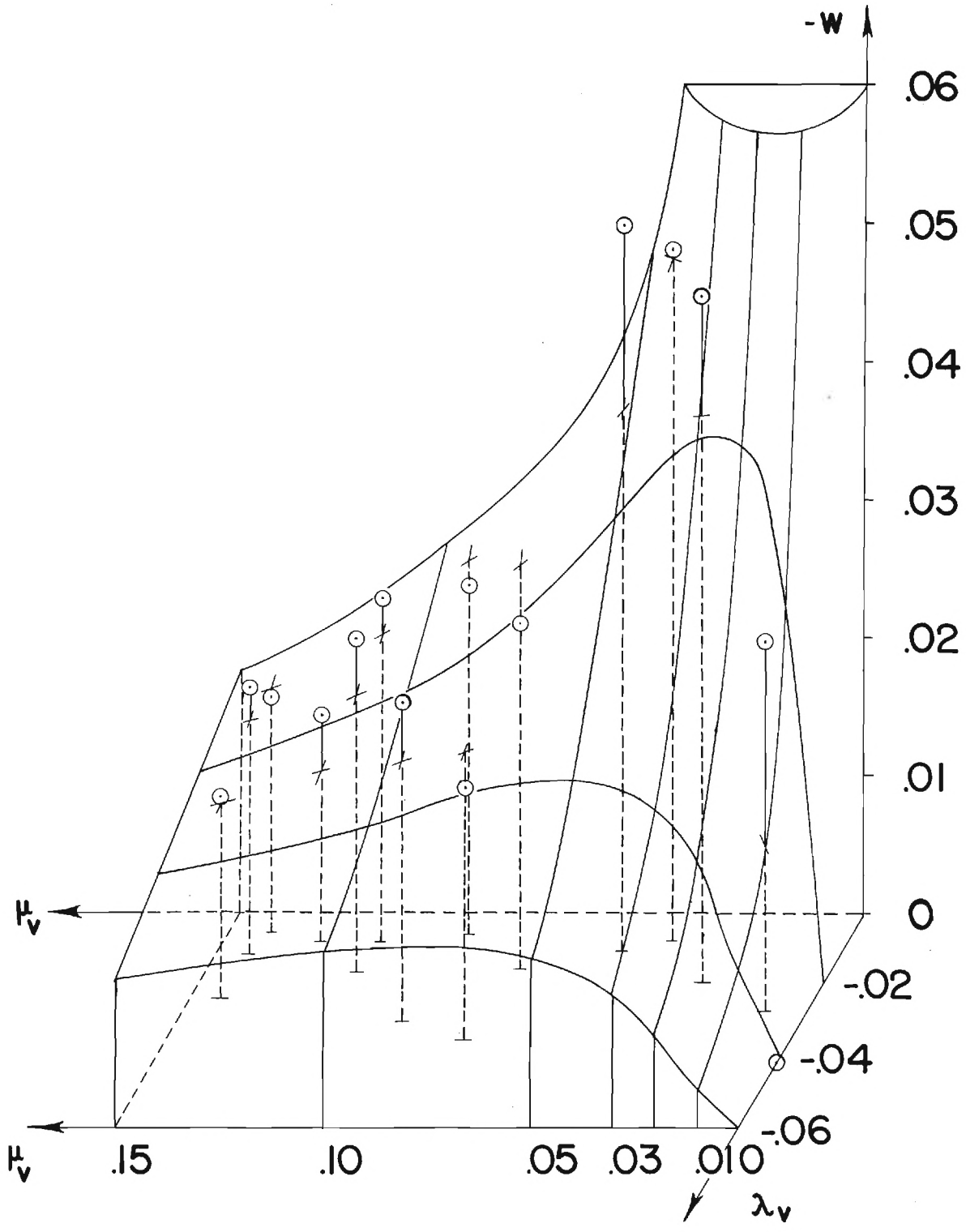

Figure 4C. Comparison of Theoretical and Experimental Values of w for $\mu_v < 1.5$, $\lambda_v < 0$.

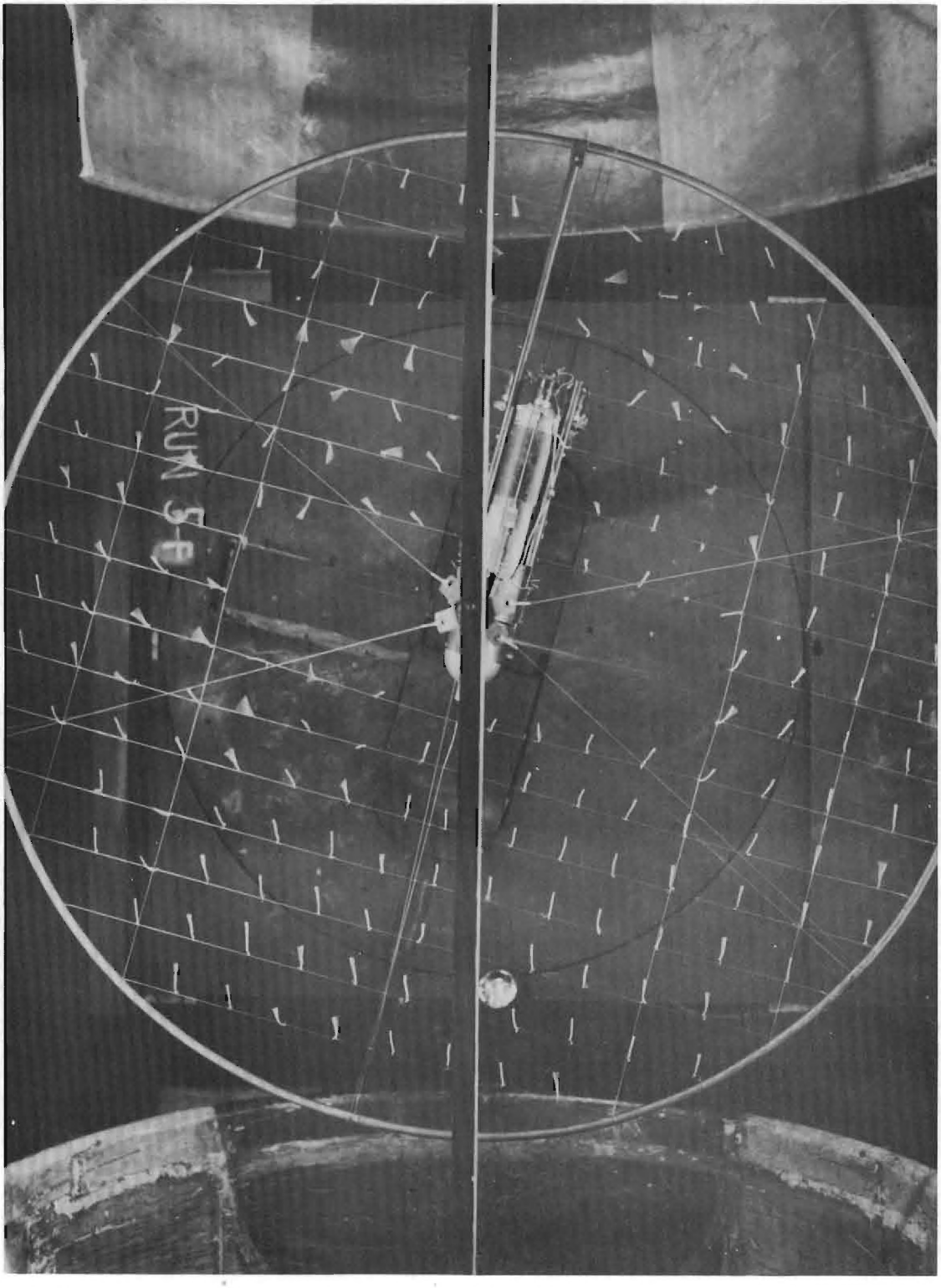

Figure 5. Photograph for Figure 7E.

Figure 6. Vertical Descent Tuft Drawings.

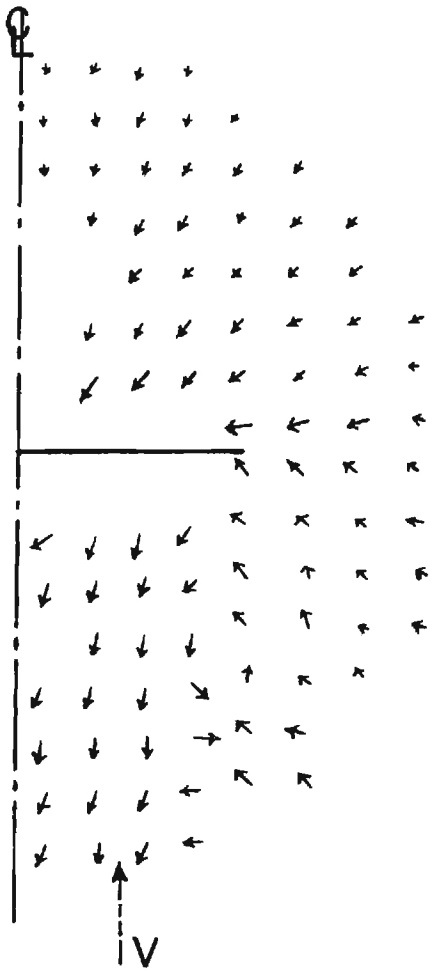

Figure 6A. $C_T = .00398$, $\frac{V}{\Omega R} = .0157$, $\lambda_z = .352$.

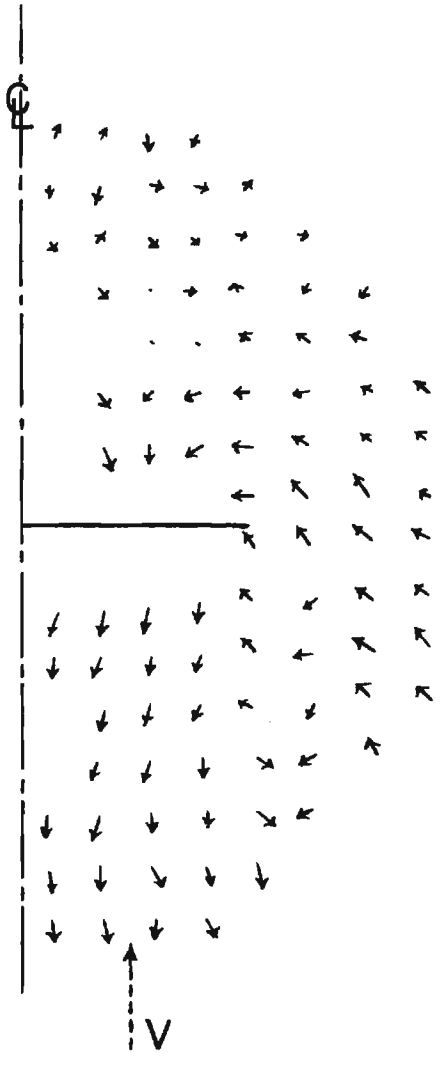

Figure 6B. $C_T = .00398$, $\frac{V}{\Omega R} = .0268$, $\lambda_z = .602$.

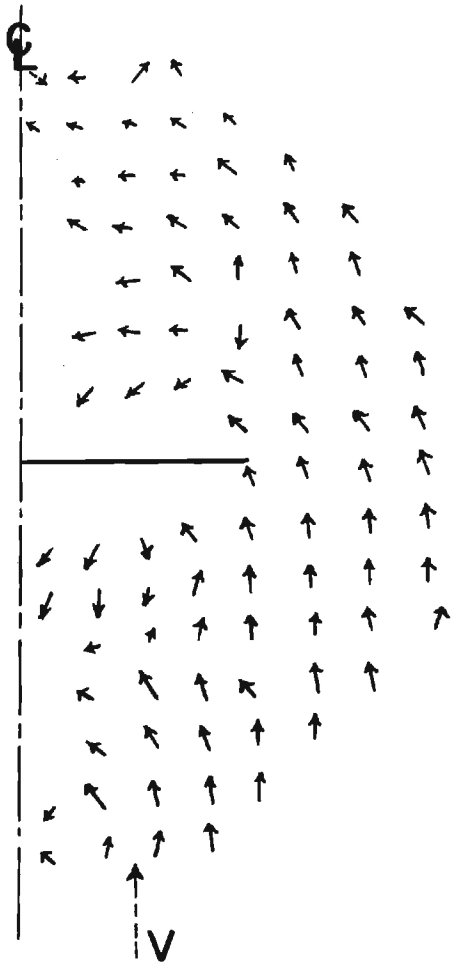

Figure 6C. $C_T = .00398$, $\frac{V}{\Omega R} = .0384$, $\lambda_z = .860$.

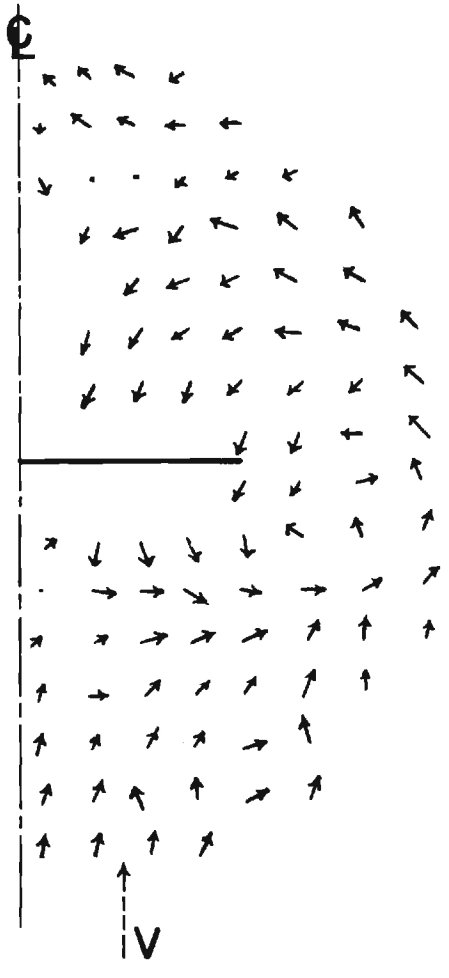

Figure 6D. $C_T = .00398$, $\frac{V}{\Omega R} = .0473$, $\lambda_z = 1.061$.

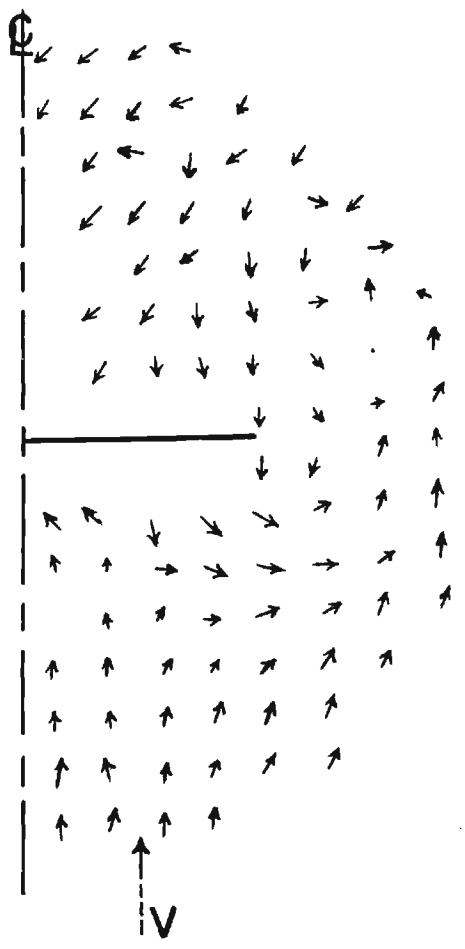

Figure 6E. $C_T = .00398$, $\frac{V}{\Omega R} = .0565$, $\lambda_z = 1.266$.

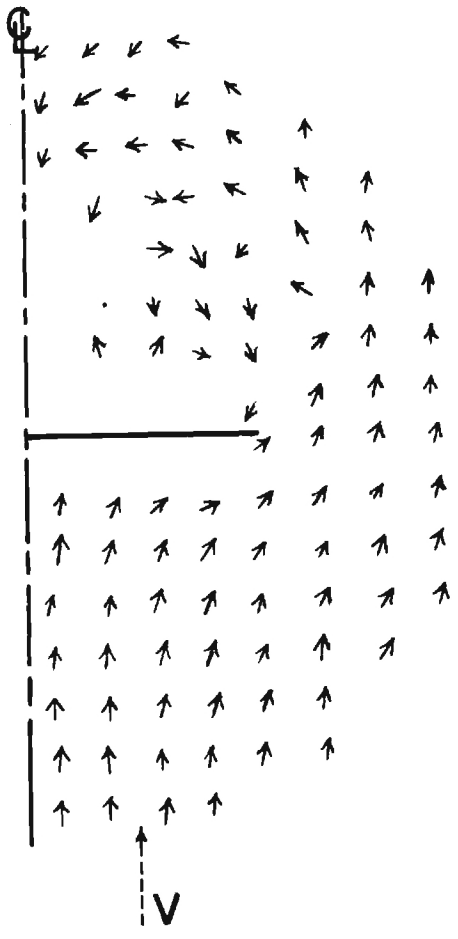

Figure 6F. $C_T = .00398$, $\frac{V}{\Omega R} = .0684$, $\lambda_z = 1.533$.

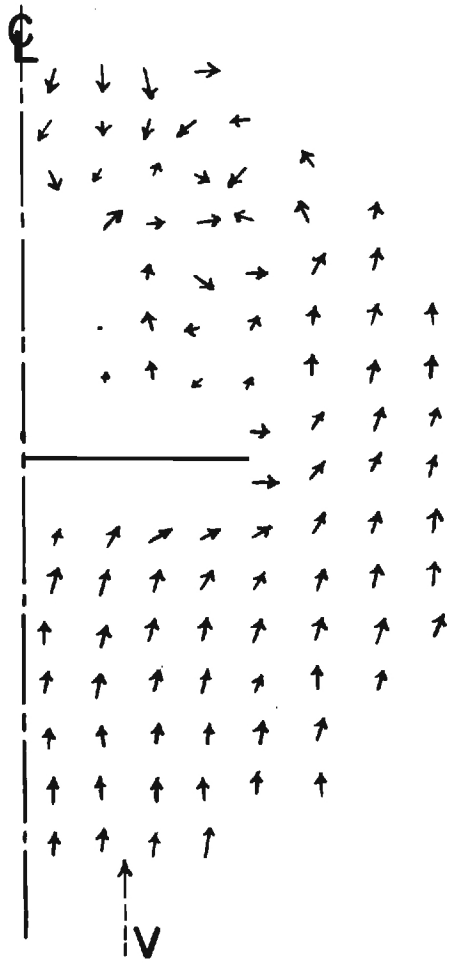

Figure 6G. $C_T = .00398$, $\frac{V}{\Omega R} = .0768$, $\lambda_z = 1.721$.

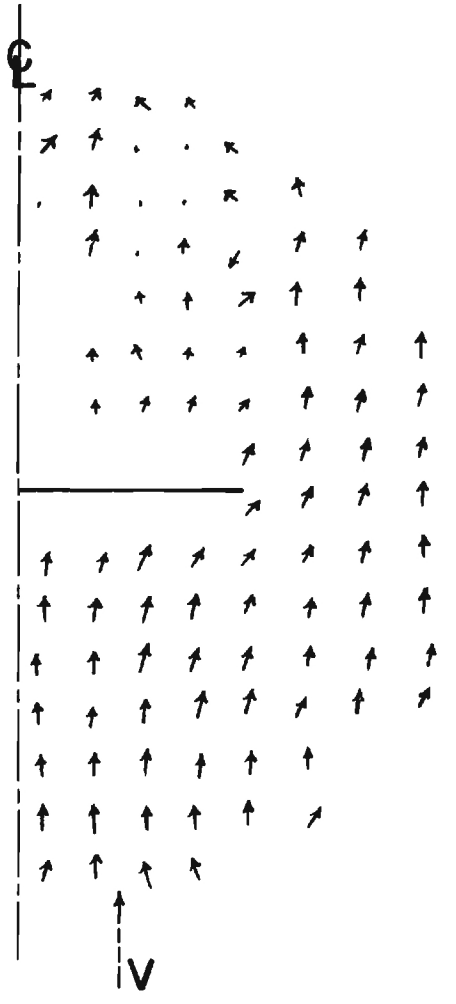

Figure 6H. $C_T = .00398$, $\frac{V}{\Omega R} = .0828$, $\lambda_z = 1.855$.

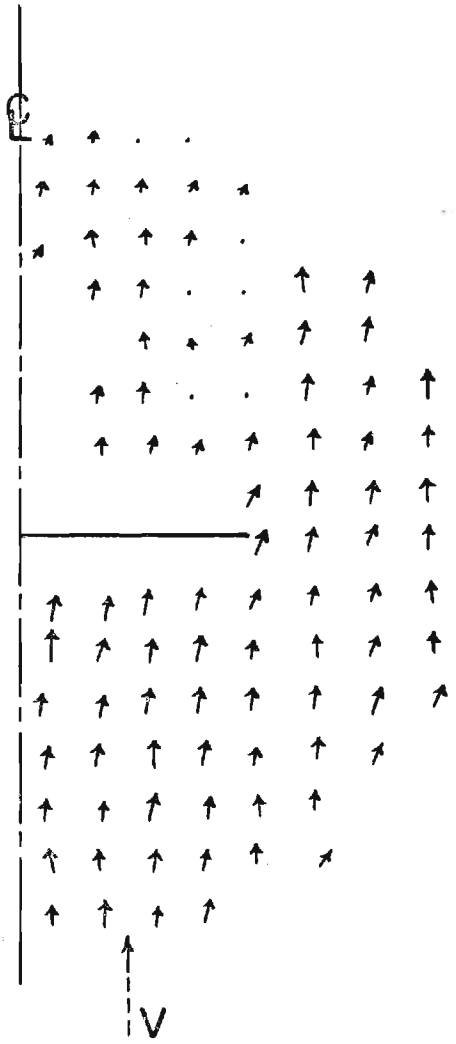

Figure 6I. $C_T = .00398, \frac{V}{\Omega R} = .0915,$ $\lambda_z = 2.051.$

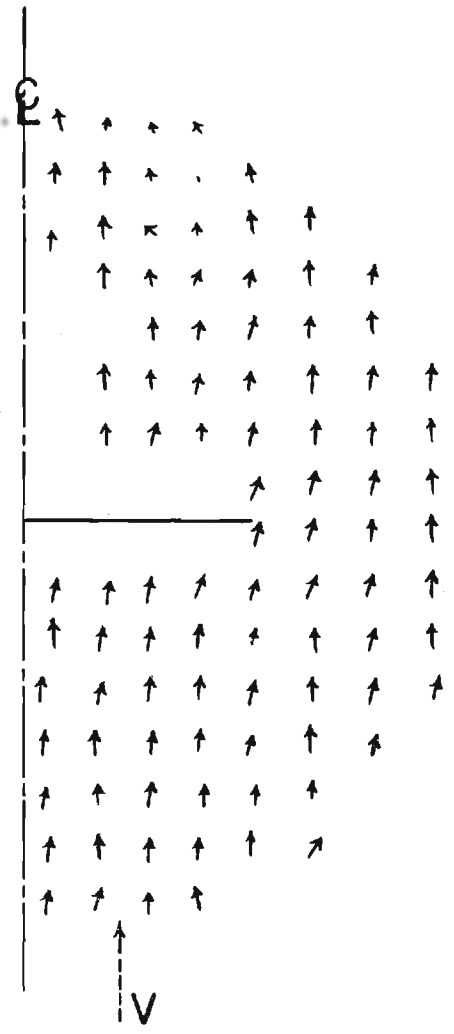

Figure 6J. $C_T = .00398, \frac{V}{\Omega R} = .0975,$ $\lambda_z = 2.184.$

Figure 7. Inclined Descent Tuft Drawings for $\frac{V}{\Omega R} = 0.075$.

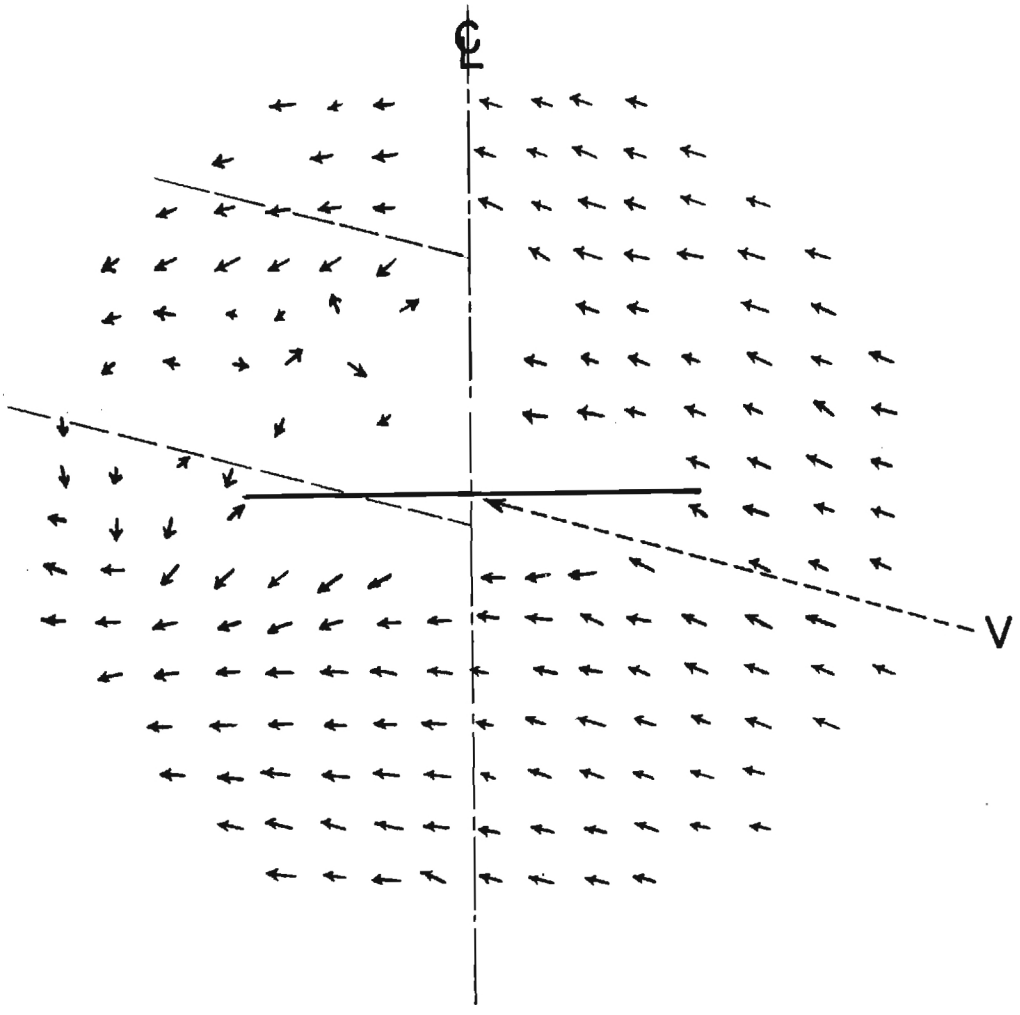

Figure 7A. $\alpha = 15^{\circ}$, $C_T = .00404$, $\frac{V}{\Omega R} = .0768$, $\lambda_x = 1.643$, $\lambda_z = .438$.

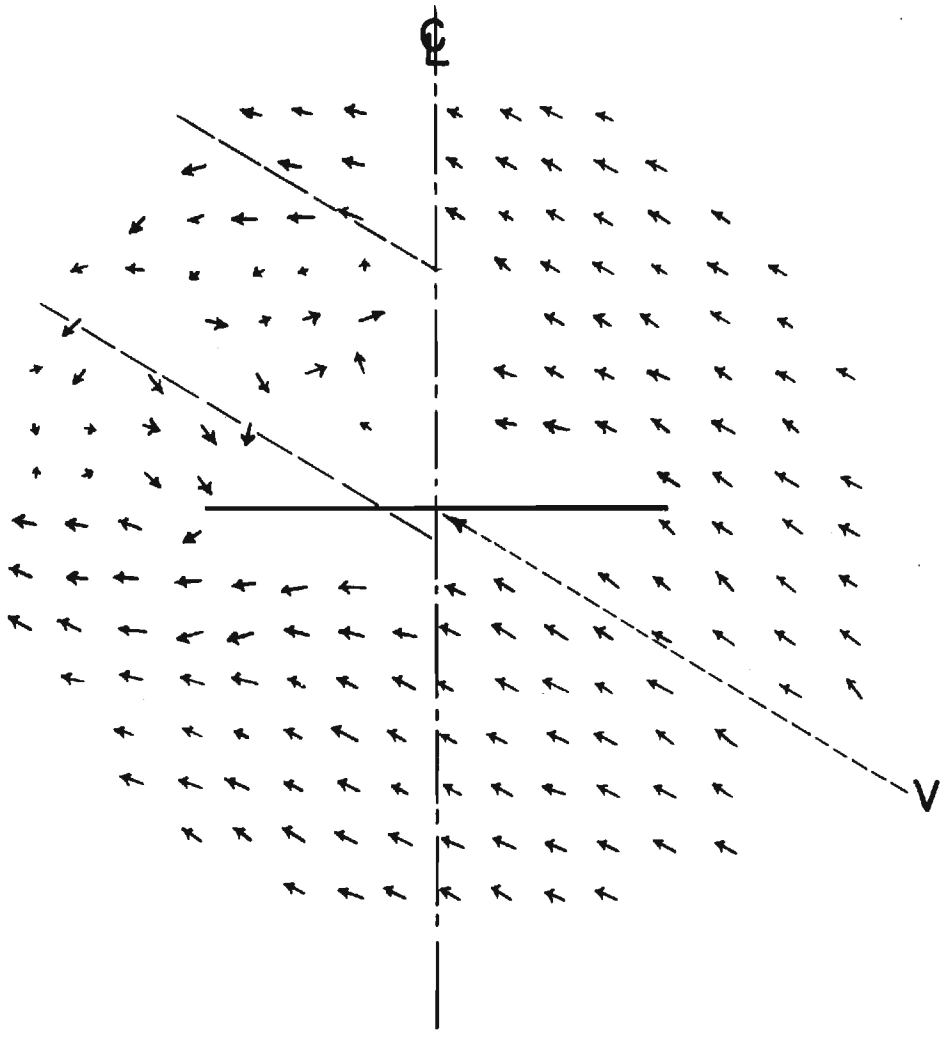

Figure 7B. $\alpha = 30^{\circ}$, $C_T = .00404$, $\frac{V}{\Omega R} = .0756$, $\lambda_x = 1.459$, $\lambda_z = .823$.

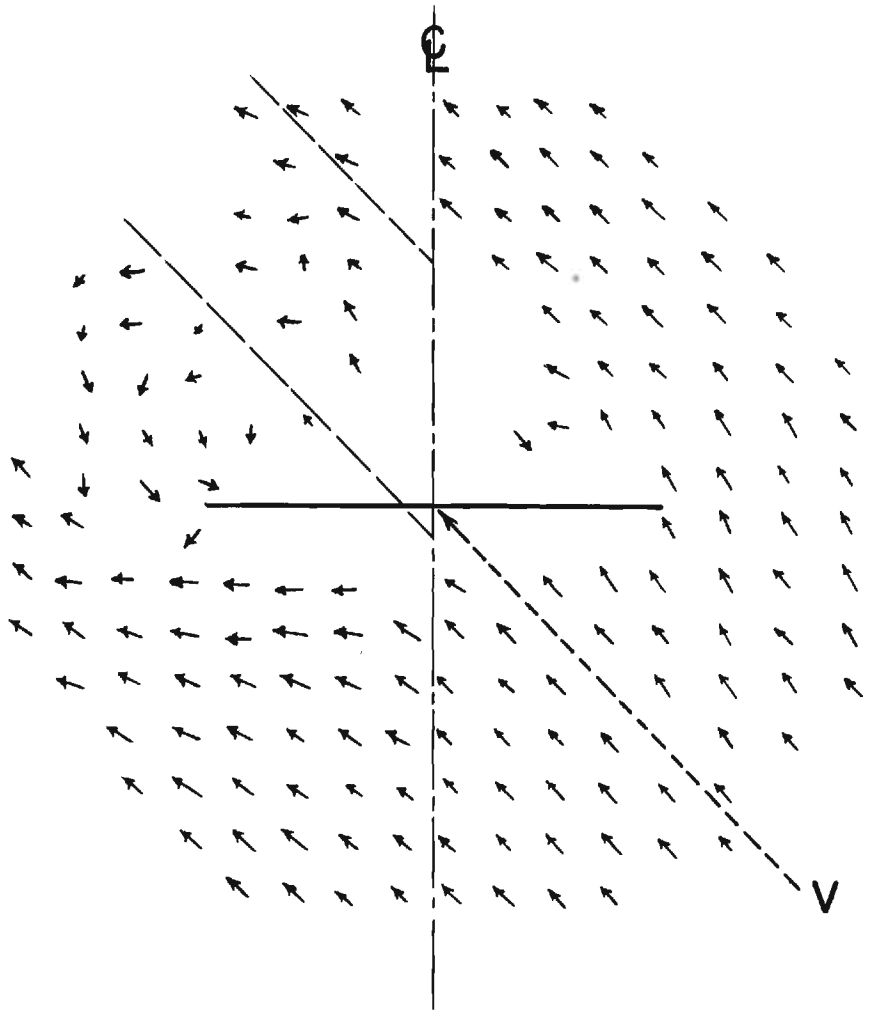

Figure 7C. $\alpha = 45^{\circ}$, $C_T = .00404$, $\frac{V}{\Omega R} = .0756$, $\lambda_x = 1.199$, $\lambda_z = 1.172$.

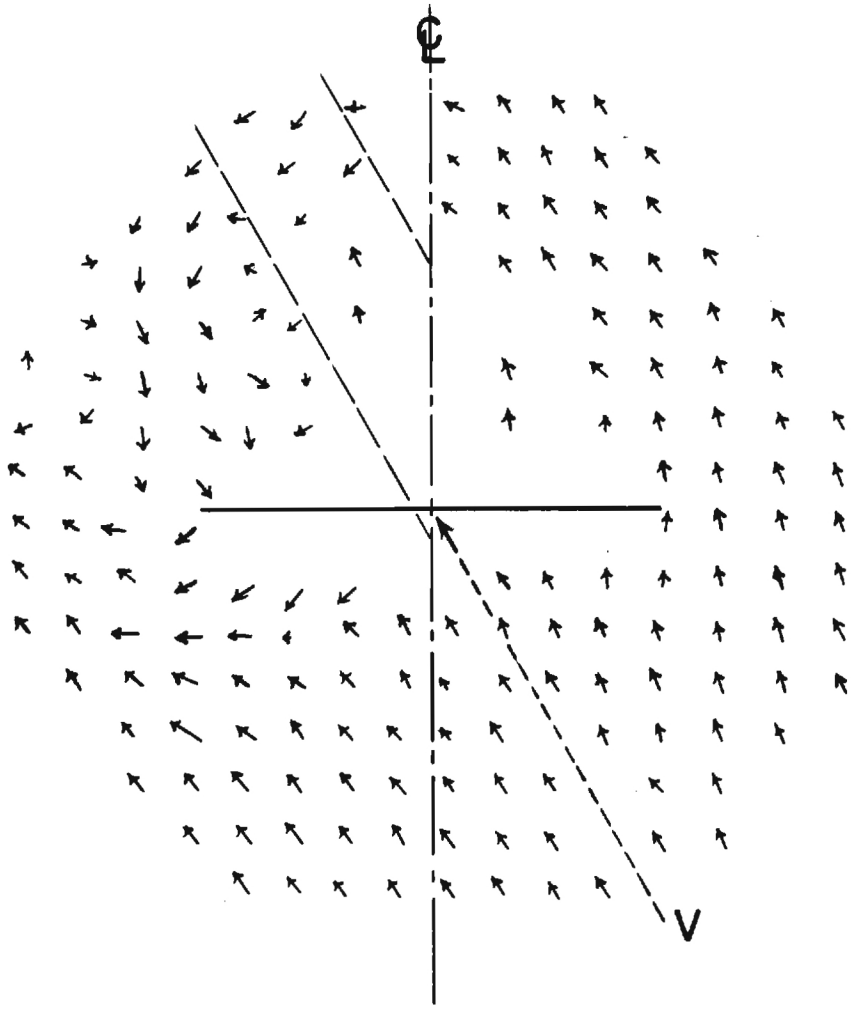

Figure 7D. $\alpha = 60^{\circ}$, $C_T = .00404$, $\frac{V}{\Omega R} = .0752$, $\lambda_x = .848$, $\lambda_z = 1.439$.

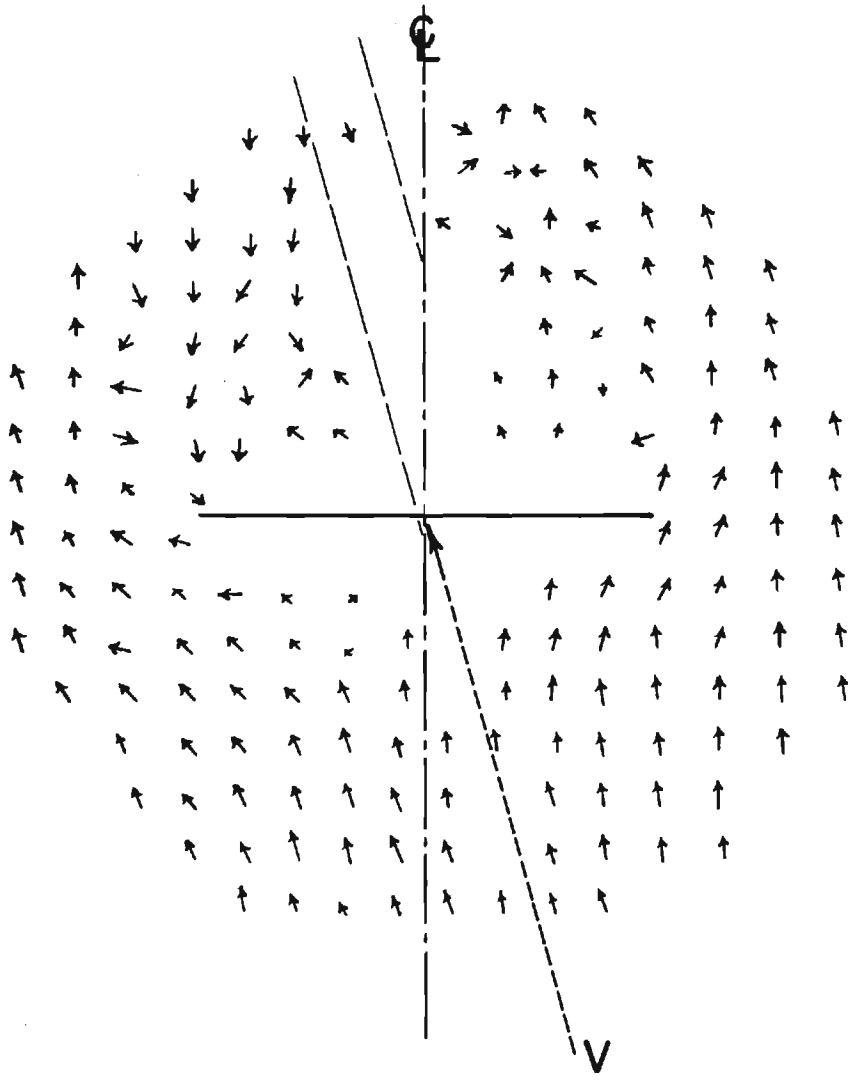

Figure 7E. $\alpha = 75^{\circ}$, $C_T = .00404$, $\frac{V}{\Omega R} = .0752$, $\lambda_x = .446$, $\lambda_z = 1.611$.

Figure 8. Inclined Descent Tuft Drawings for $\frac{V}{\Omega R} = 0.16$.

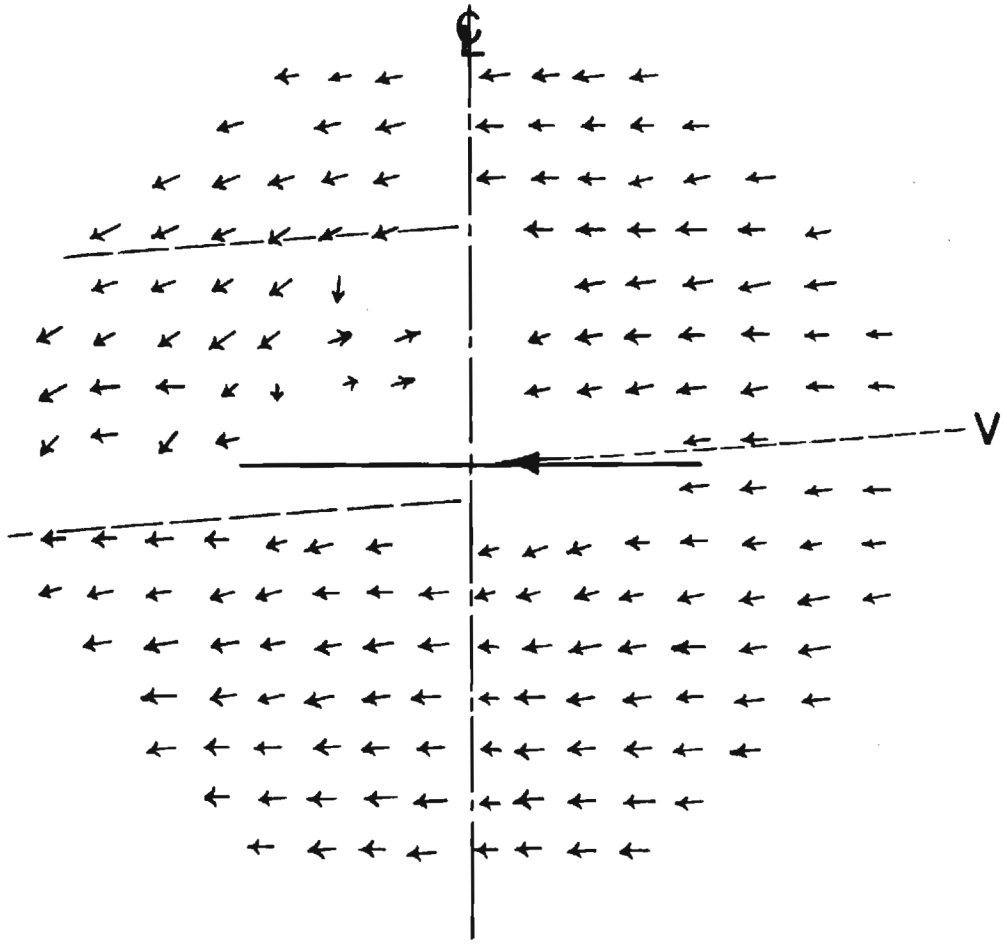

Figure 8A. $\alpha = -5^{\circ}$, $C_T = .00416$, $\frac{V}{\Omega R} = .1619$, $\lambda_x = 3.475$, $\lambda_z = -.125$.

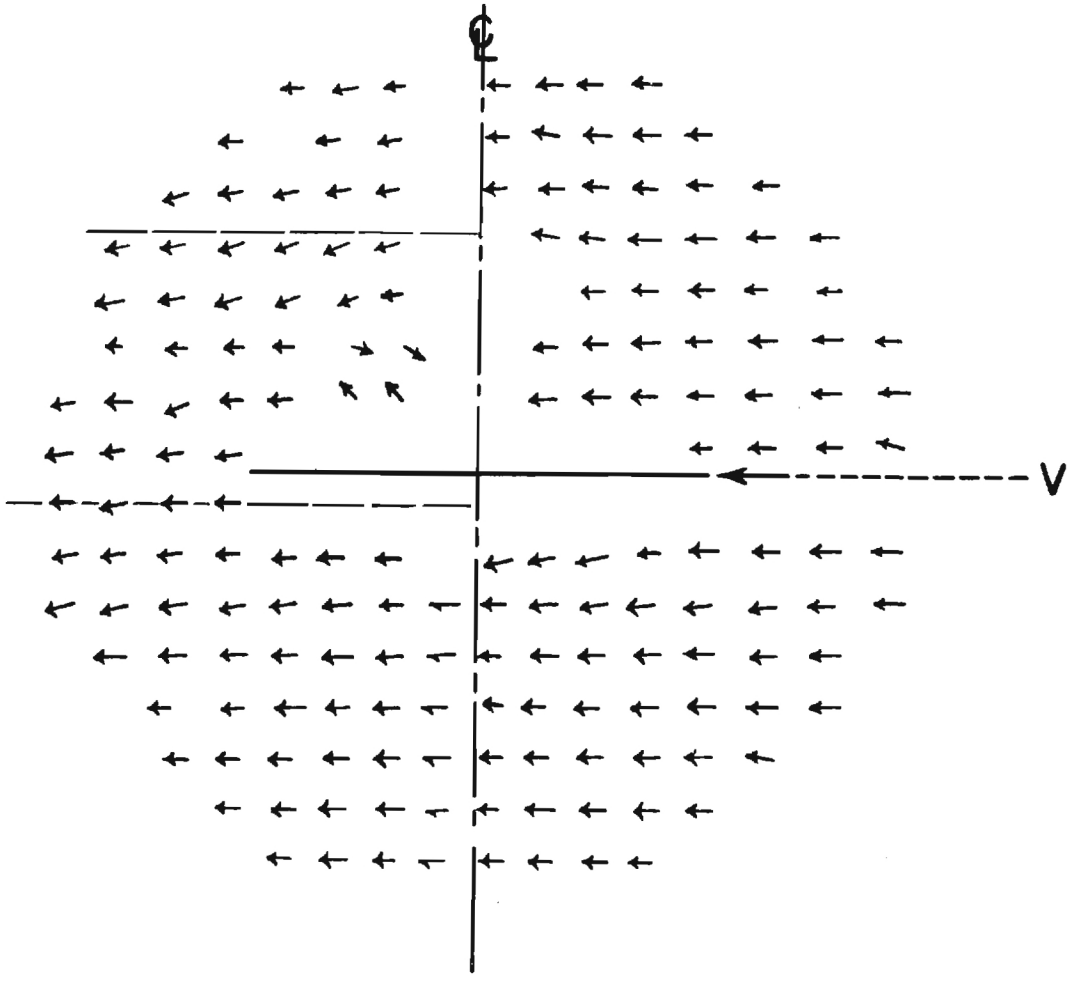

Figure 8B. $\alpha = 0^{o}$, $C_T = .00416$, $\frac{V}{\Omega R} = .1615$, $\lambda_x = 3.466$, $\lambda_z = .162$.

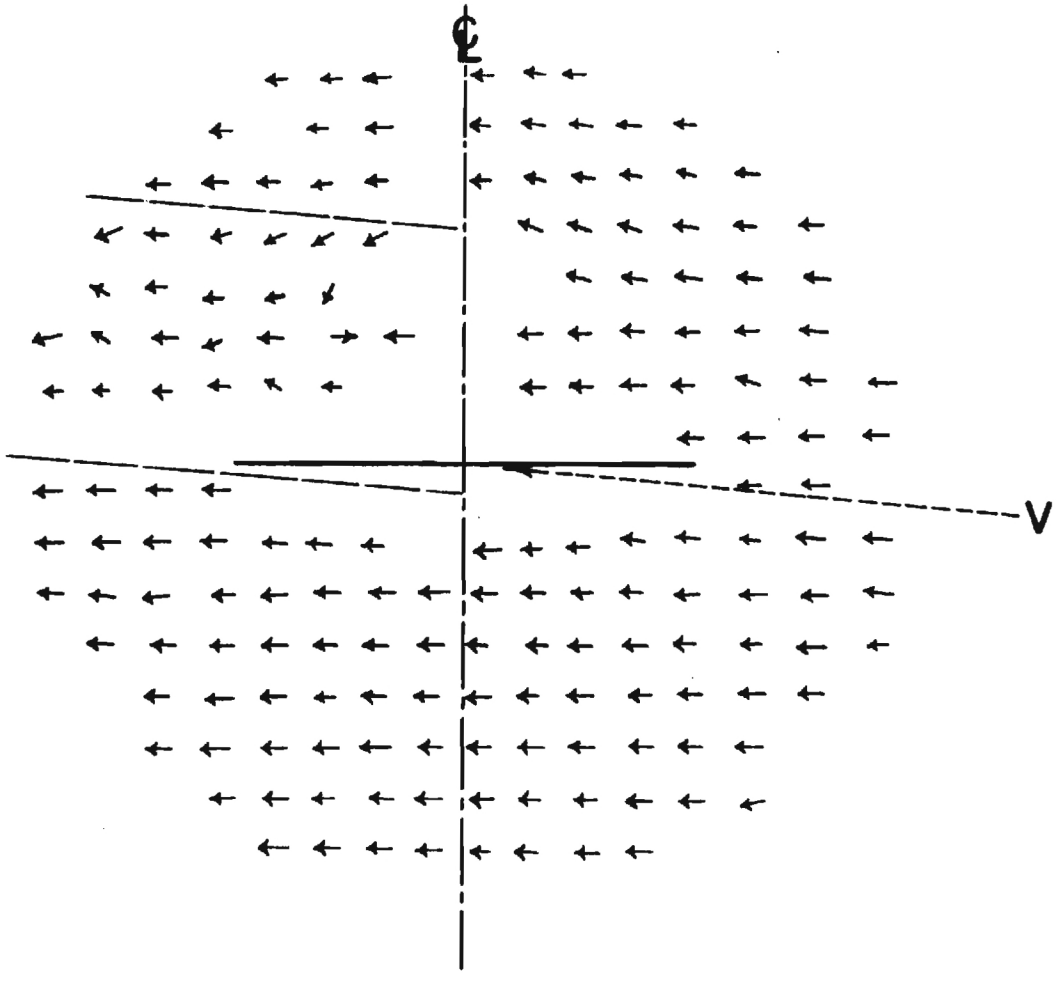

Figure 8C. $\alpha = 5^{\circ}$, $C_T = .00416$, $\frac{V}{\Omega R} = .1615$, $\lambda_x = 3.444$, $\lambda_z = 423$.

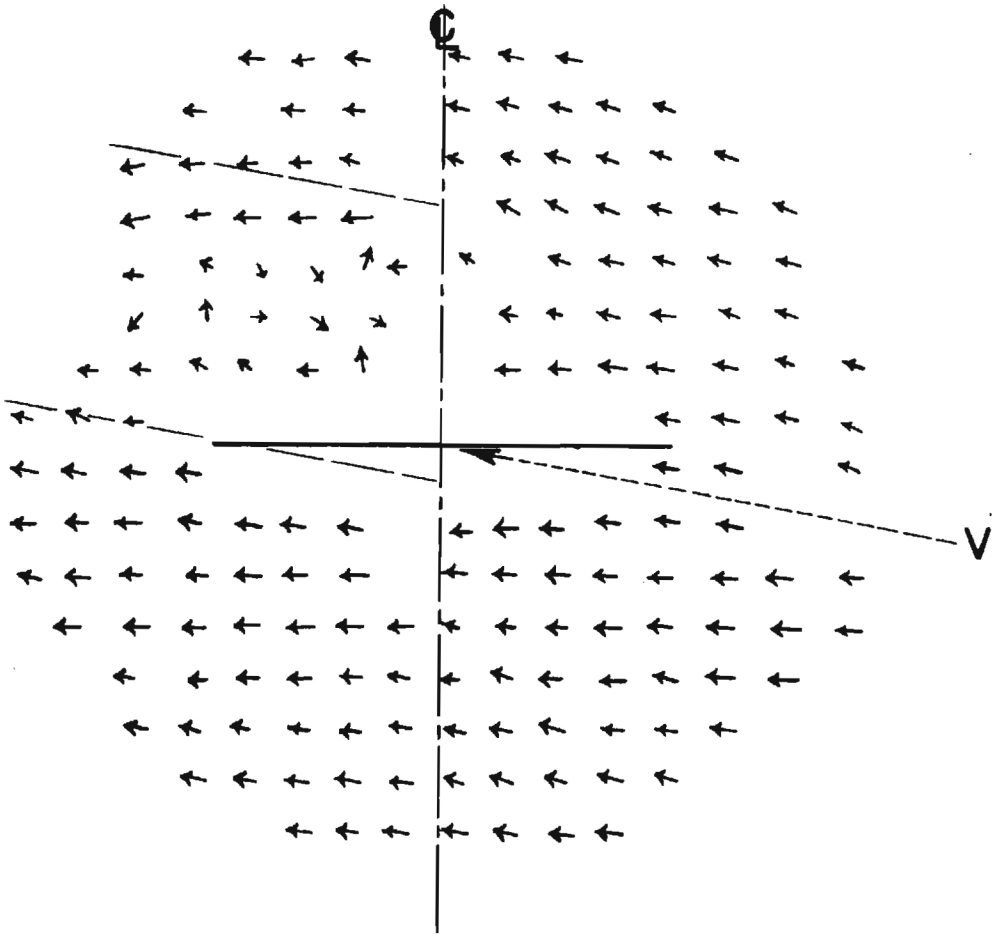

Figure 8D. $\alpha = 10^{\circ}$, $C_T = .00416$, $\frac{V}{\Omega R} = .1615$, $\lambda_x = 3.403$, $\lambda_z = .691$.

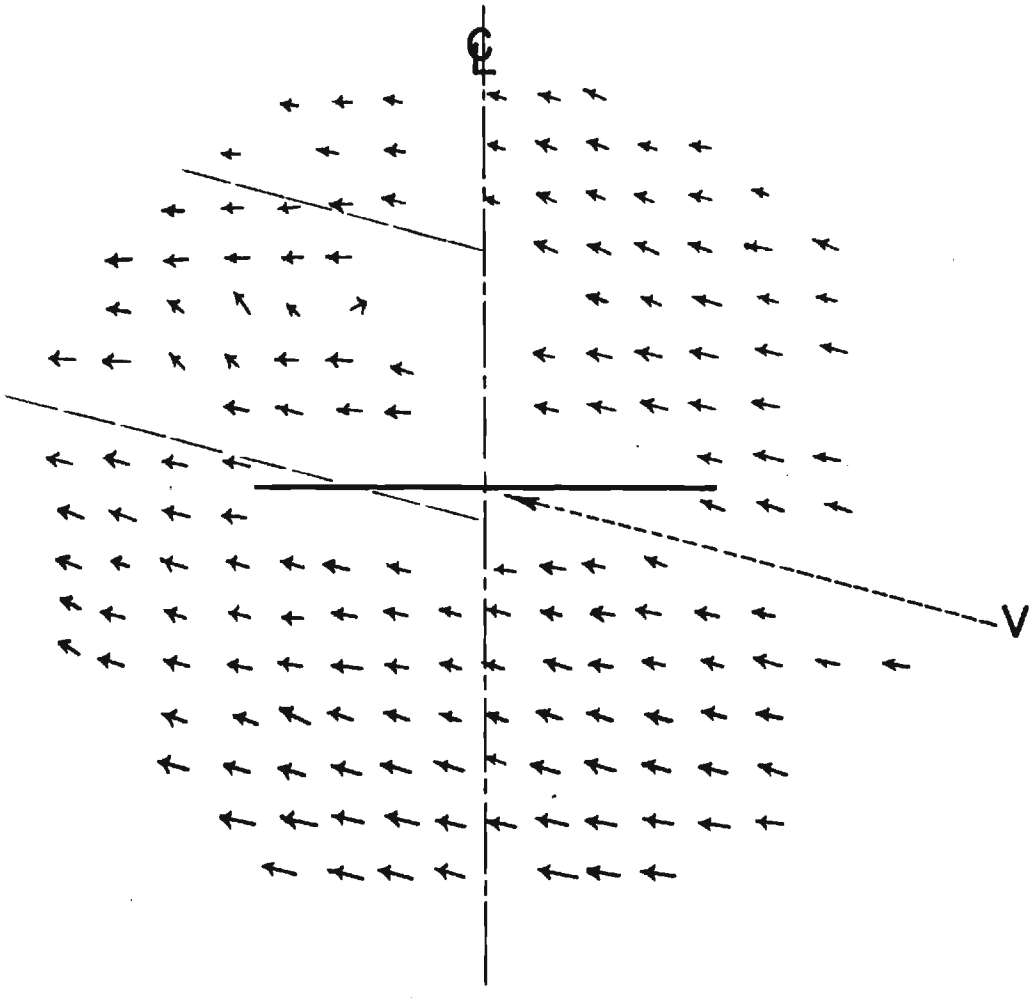

Figure 8E. $\alpha = 15^{\circ}$, $C_T = .00416$, $\frac{V}{\Omega R} = .1615$, $\lambda_x = 3.337$, $\lambda_z = .968$.

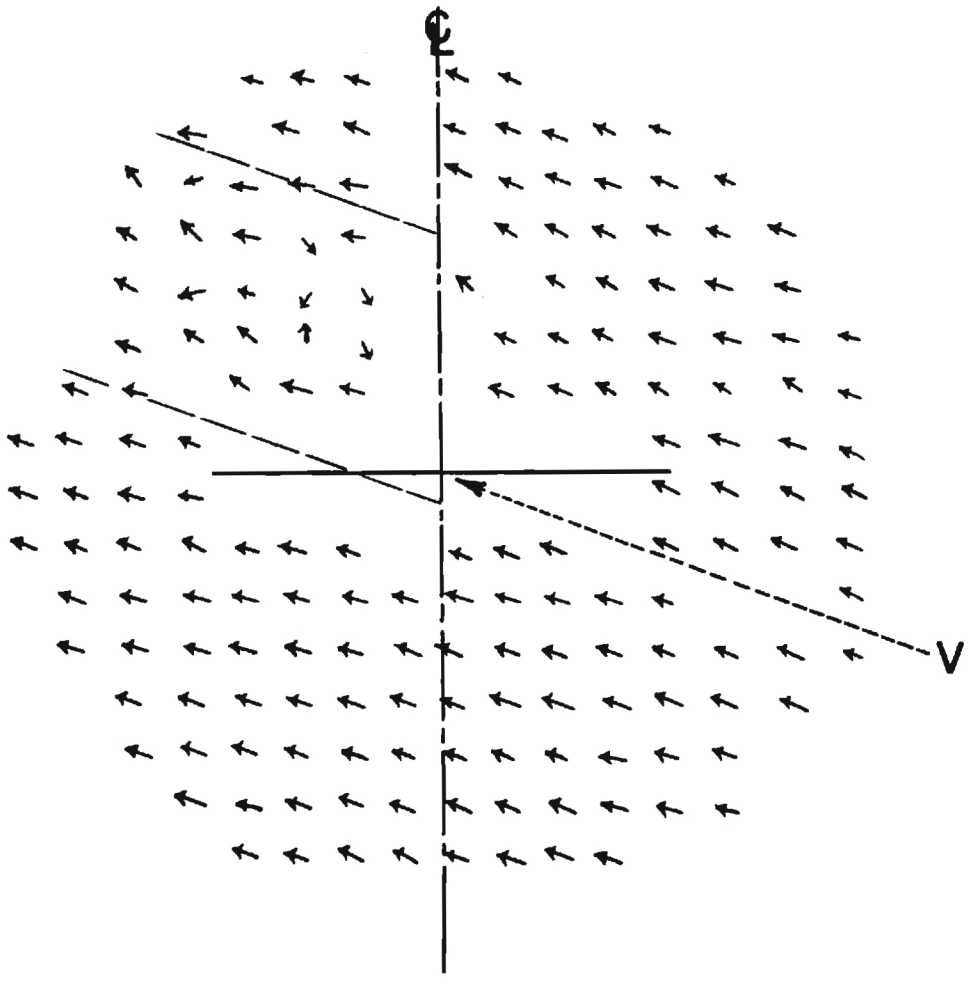

Figure 8F. $\alpha = 20^{o}$, $C_T = .00416$, $\frac{V}{\Omega R} = .1615$, $\lambda_x = 3.249$, $\lambda_z = 1.240$.

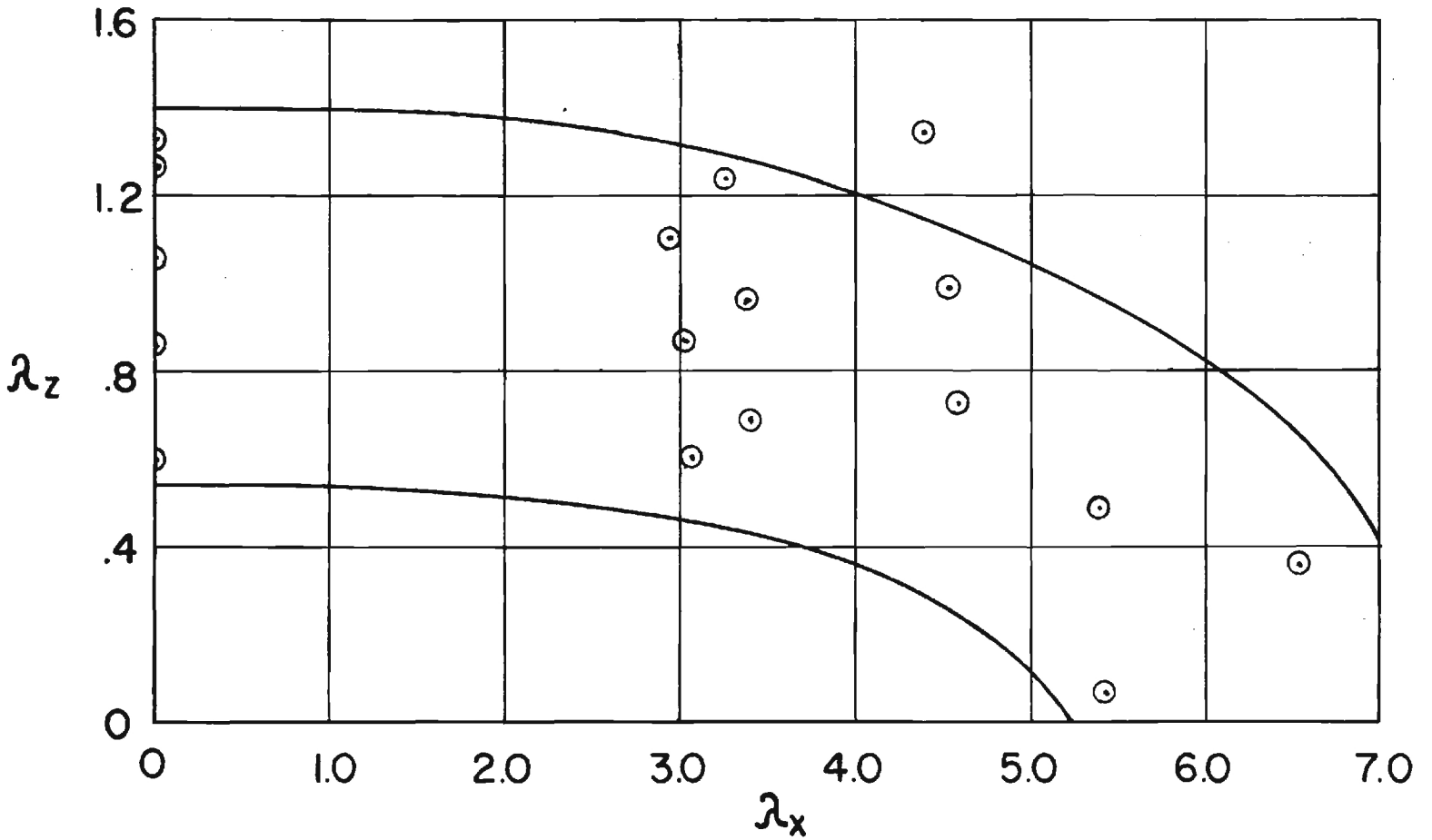

Figure 9. Region of Rough Flow.

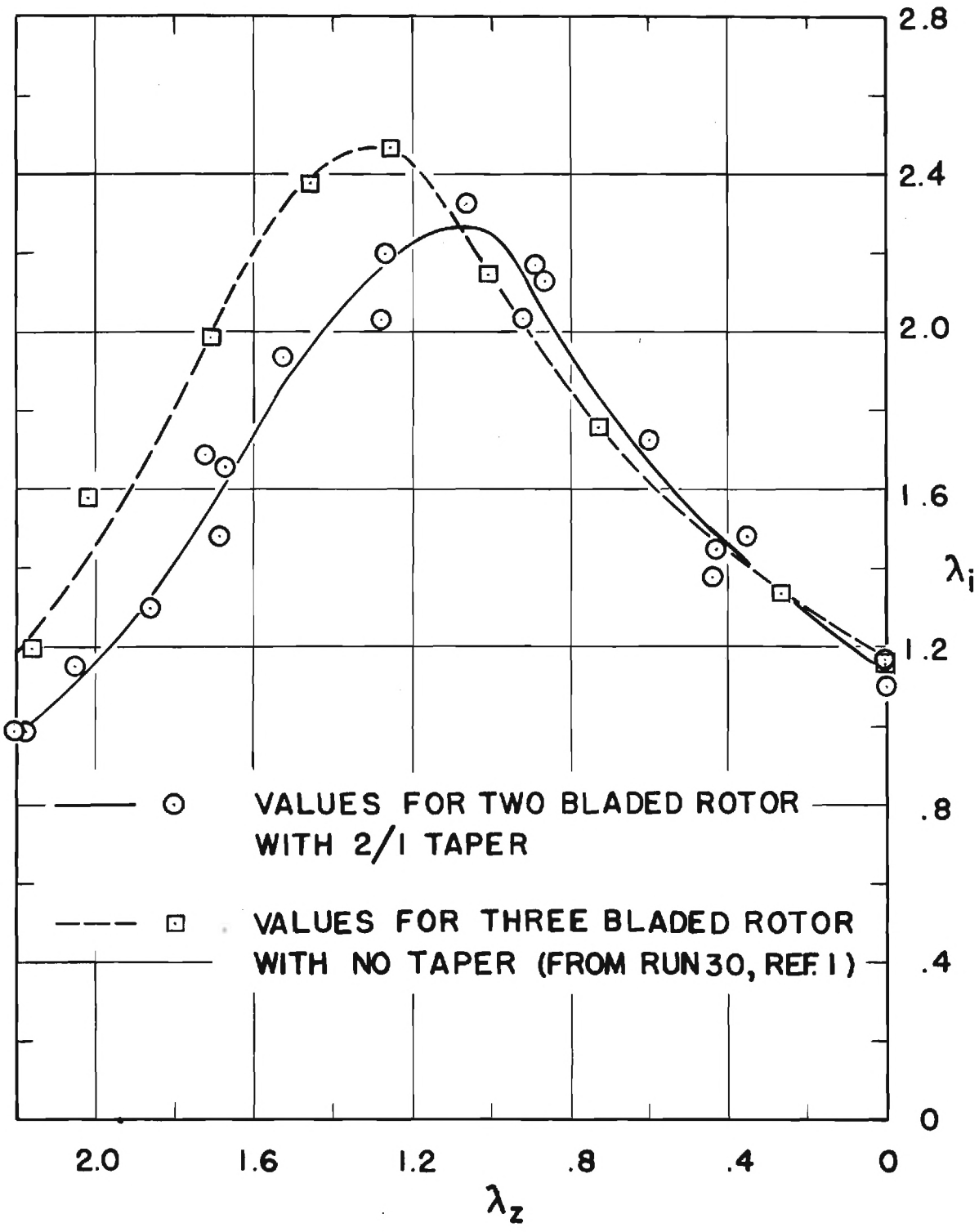

Figure 10. λ_i Versus λ_z for Vertical Descent.